Although the biological significance of this clustering of highly expressed, organ-related genes along the chromosomes is not clear, these clusters must provide significant advantages for tissue-specific functioning. The functional annotation of liver-related chromosomal domains revealed that they encoded metabolism-related genes such as for xenobiotic, lipid, and alcohol metabolism. The lipid and alcohol metabolism is liver specific. The functional annotation of colon-related chromosomal domains revealed that they encoded apoptosis, cell proliferation, ion transporter, and mucin production. These functions are essential for colon epithelium producing gut fluid and compatible with the short life span of the colon epithelium [9,10]. Thus, we first identified the presence of organ-related gene clusters in chromosomes and revealed their biological significance for organ-specific functioning.

In general, the relative proportions of cell types differ in each organ and affect the patterns of gene expression. In this study, we identified six liver-related and five colon-related chromosomal domains, whereas no brain-related or breast-related chromosomal domains were found on whole chromosome. It is possible that different compositions of cells might underestimate the presence of organ-related gene clusters in chromosomes.

What is the biological and evolutionary background of these organ-related chromosomal domains? In general, transcriptional machineries may access two coexpressed genes more efficiently when they are neighbors, so active transcription of organ-related chromosomal domains may result from the binding of a specific transcription factor to these domains [2]. Another possibility is that the formation of organ-related chromosomal domains in the human genome is the result of chromosome rearrangement during the process of evolution, because the organ-related chromosomal domains were conserved in one or two mouse and rat chromosomes. Recent comparative analyses of large-scale genome sequencing revealed that rearrangement of chromosomal segments and localized duplication of genomic segments are two major factors in eukaryotic genome evolution [11]. Our data revealed that half of the organ-related chromosomal domains contained multigene families. These results suggest that the gene duplications may also contribute to the formation of organ-specific functionality in mammalian evolution.

Recently, draft genome sequences of the Brown Norway rat were analyzed and compared with the human and mouse genomes, revealing that the human and rodent genomes contain conserved synteny blocks [12]. We therefore investigated the organ-related chromosomal domains with reported conserved synteny blocks in human, mouse, and rat genomes (http://www.genboree.org) and identified that all organ-related chromosomal domains were included in synteny blocks conserved in human and rodent genomes (data not shown). These data might indicate the proximity of the human and rodent genomes in mammalian evolution, and organ-related chromosomal domains may have constituted parts of synteny blocks of larger size during human, mouse, and rat genome evolution.

If the number of genes in a chromosomal domain were small and the transcriptional activity in most of a tissue were low in the 5-Mb window, we could not eliminate the effects of a single highly expressed gene on the TDF score. To eliminate this limitation, we set the region criteria of gene density to more than two genes in a window of 1 Mb. Another limitation of the method is the inability to reveal some chromosomal domains with equal up–down differential gene expression. Although the method in this study still has some limitations, our data could provide the candidate organ-related chromosomal domains and could highlight the neighboring genes on the domains with tissue specificity.

In conclusion, we have identified gene expression patterns along the chromosomes in normal human liver, brain, breast, and colon, showing the clustering of organ-related genes on specific chromosomal domains. Our results indicate that the human genome organization may be closely related to the organ-specific gene expression patterns.

Materials and methods

SAGE

To determine organ-specific gene expression patterns comprehensively along human chromosomes, we collected SAGE databases derived from normal tissues. To avoid individual variations in gene expression, we selected, for each tissue, SAGE libraries that contained at least 50,000 tags, and we used at least two libraries per tissue type. We analyzed publicly available SAGE libraries derived from normal brain (GSM676, GSM695), breast (GSM677, GSM780, GSM781), and colon (GSM728, GSM729) tissues (ftp://ftp.ncbi.nih.gov/pub/sage/). We also constructed SAGE libraries derived from normal liver tissues (http://www.intmedkanazawa.jp/) [13], as well as reference SAGE databases containing publicly available normal human brain, breast, colon, heart, kidney, liver, lung, prostate, and stomach SAGE libraries (GSM761, GSM677, GSM728, GSM1499, GSM708, GSM785, GSM762, GSM739, GSM739, and GSM784), each containing about 50,000 SAGE tags. All sequence files from these databases were analyzed with SAGE 2000 software, kindly donated by Drs. Kenneth W. Kinzler and Bert Vogelstein. The number of SAGE tags per library was normalized to 450,000 transcripts.

Transcriptome mapping

Gene identity and UniGene CLUSTER assignment of each SAGE tag were obtained from the SAGEmap reliable tag-to-gene mapping table (http://www.sagenet.org/SAGEDatabases/unigene.htm). Association of UniGene

clusters with chromosome positions was obtained from RefSeq build 31 (http://www.ncbi.nlm.nih.gov/RefSeq/) and LocusLink (http://www.ncbi.nlm.nih.gov/LocusLink/) databases (November 26, 2002). SAGE tag locations along the chromosomes were matched to physical distance information by connecting the SAGE map, RefSeq, and LocusLink tables with the UniGene number.

Transcription density and gene density

Transcriptional activity was determined from the TDF [7]. Briefly, TDF is calculated using a 5-Mb window moving along the chromosome at 1-Mb intervals and defined as TDF = $\ln(R/R_{\mathrm{ref}})/(T/T_{\mathrm{ref}})$, where R is the number of SAGE tags in each library and T is the number of unique SAGE tags in each library, within a window of 5 Mb. Gene density is defined as the number of RefSeq records divided by the average RefSeq records in each 5-Mb window. The correlation between transcription density and gene density in each chromosome was assessed by calculating the Pearson's correlation coefficient using the equation

$$r=\frac{n\left(\sum_{i=1}^{n} XiYi\right)-\left(\sum_{i=1}^{n} Xi\right)\left(\sum_{i=1}^{n} Yi\right)}{\sqrt{\left\{n\sum_{i=1}^{n} Xi^2-\left(\sum_{i=1}^{n} Xi\right)^2\right\}\left\{n\sum_{i=1}^{n} Yi^2-\left(\sum_{i=1}^{n} Yi\right)^2\right\}}}$$

where X_i is the number of SAGE tags in each library and Y_i is the number of RefSeq records in each 5-Mb window.

To investigate the statistical significance of the TDF values selected, we performed a permutation test. The following argument explains a statistical method that tests the null hypothesis that two groups are equivalent in the distribution of orders of their members. The alternative hypothesis is that members of one of the groups tend to rank higher. By rejecting the null hypothesis, we show that selected members are significantly high-ranked in the order of a variable. First we set up the notation. Suppose that n regions are classified into two groups. Each region is indexed by i, where $i \in I := \{1,2,\ldots,n\}$ and I_1 denotes the set of indices of the first group of m regions. Assuming that an observed value x_i is attributed to the ith region, we denote the order statistics of the values by $x_{(1)} > x_{(2)} > \ldots > x_{(n)}$, where no tie is assumed to simplify the argument. Let a function $\rho(i)$, $i \in I$ uniquely assign to an index its rank: $x_i = x_{(\rho(i))}$.

A permutation test is adopted, and without loss of generality, we henceforth assume that $I_1 = \{1, 2, \ldots, m\}$. Under the null hypothesis,

$$Pr(\rho(1)) = i_1, \rho(2) = i_2,\ldots, \rho(m) = i_m) = \frac{1}{\binom{n}{m}}$$

for all the elements of $\{(i_1,i_2,..i_m)\in I^m \mid \forall j\neq k, i_j\neq i_k, (j,k)\in I_1^2\}$.

Let us consider the test statistic $T = \sum_{i=1}^{m} \rho(i)$ where the null hypothesis is rejected for some c if $T < c$. Consequently, the p value of a realized test statistic t is given by $Pr(T \leq t)$. In particular, if the regions of the first group are ranked from the first to the mth, the p value reduces to

$$Pr\left(T \leq \frac{m(1+m)}{2}\right) = \frac{1}{\binom{n}{m}}$$

To be concrete, let us regard x_i as the TDF of the ith region, for example. Top m ranks group together under the criterion that selects the regions where TDFs are larger than 1.8. Hence its significance is easy to evaluate by the aforesaid method, and the rejection of the null hypothesis implies that the selected regions' TDFs are larger. Similarly, if we select the regions where an objective organ's TDF is larger than 1.8 and other organs' TDFs are smaller than 1.0, just regard x_i as the number of organs whose TDFs are smaller than 1.0. Then top m ranks consist of the selected regions among n regions where an objective organ's TDF is larger than 1.8. In this case, the rejection of the null hypothesis implies that the TDFs of organs other than the objective are relatively small in the selected regions.

Comparison of organ-related chromosomal domains in rat, mouse, and human genomes

All genes located on organ-related chromosomal domains in human were listed using the RefSeq build 31 database (http://www.ncbi.nlm.nih.gov/RefSeq/). All possible homologous genes and their locations on the *R. norvegicus* and *M. musculus* genomes were searched using the HomoloGene database (February 20, 2004) (http://www.ncbi.nlm.nih.gov/entrez/query.fcgi?DB=homologene). The chromosomal location and the gene list on each domain were also confirmed by MapViewer (http://www.ncbi.nlm.nih.gov/mapview/).

Pathway analysis

To investigate the functions of genes located on organ-related chromosomal domains comprehensively, we used PathwayAssist software (Ariadone Genomics, Rockville, MD, USA). All genes located on the chromosomal domains were investigated and annotated with the biological processes, protein–protein interactions, and gene regulatory networks using a reference-based data file.

Acknowledgment

The authors thank Dr. Koichi Miwa for providing human liver tissues.

References

[1] H. Caron, et al., The human transcriptome map: clustering of highly expressed genes in chromosomal domains, Science 291 (2001) 1289–1292.
[2] P.J. Roy, J.M. Stuart, J. Lund, S.K. Kim, Chromosomal clustering of muscle-expressed genes in Caenorhabditis elegans, Nature 418 (2002) 975–979.
[3] P.T. Spellman, G.M. Rubin, Evidence for large domains of similarly expressed genes in the Drosophila genome, J. Biol. 1 (2002) 5.
[4] G.M. Rubin, et al., Comparative genomics of the eukaryotes, Science 287 (2000) 2204–2215.
[5] H. Abderrahim, et al., Cloning the human major histocompatibility complex in YACs, Genomics 23 (1994) 520–527.
[6] K. Omori, L. Vergnes, M.M. Zakin, A. Ochoa, The apolipoprotein AICIII–AIV gene cluster: sequence of the ApoCIII–ApoAIV intergenic region, Gene 159 (1995) 231–234.
[7] P. Qiu, L. Benbow, S. Liu, J.R. Greene, L. Wang, Analysis of a human brain transcriptome map, BMC Genom. 3 (2002) 10.
[8] J.D. Barrans, et al., Chromosomal distribution of the human cardiovascular transcriptome, Genomics 81 (2003) 519–524.
[9] K. Kunzelmann, M. Mall, Electrolyte transport in the mammalian colon: mechanisms and implications for disease, Physiol. Rev. 82 (2002) 245–289.
[10] P. de Santa Barbara, G.R. van den Brink, D.J. Roberts, Development and differentiation of the intestinal epithelium, Cell. Mol. Life Sci. 60 (2003) 1322–1332.
[11] E.E. Eichler, D. Sankoff, Structural dynamics of eukaryotic chromosome evolution, Science 301 (2003) 793–797.
[12] R.A. Gibbs, et al., Genome sequence of the Brown Norway rat yields insights into mammalian evolution, Nature 428 (2004) 493–521.
[13] T. Yamashita, et al., Comprehensive gene expression profile of a normal human liver, Biochem. Biophys. Res. Commun. 269 (2000) 110–116.

[CANCER RESEARCH 64, 3326–3333, May 1, 2004]

Different Procarcinogenic Potentials of Lymphocyte Subsets in a Transgenic Mouse Model of Chronic Hepatitis B

Yasunari Nakamoto,[1] Takashi Suda,[2] Takashi Momoi,[3] and Shuichi Kaneko[1]

[1]Department of Gastroenterology, Graduate School of Medicine, [2]Center for the Development of Molecular Target Drugs, Cancer Research Institute, Kanazawa University, Kanazawa, and [3]Division of Development and Differentiation, National Institute of Neuroscience, NCNP, Kodaira, Tokyo, Japan

ABSTRACT

The immune response to hepatitis viruses is believed to be involved in the development of chronic hepatitis; however, its pathogenetic potential has not been clearly defined. The current study, using a transgenic mouse model of chronic hepatitis B, was designed to determine the relative contributions of the immune cell subsets to the progression of liver disease that induces hepatocellular carcinogenesis. Hepatitis B virus transgenic mice were adoptively transferred with $CD4^+$ and $CD8^+$ T cell-enriched or -depleted and B cell-depleted splenocytes obtained from hepatitis B surface antigen-primed, syngeneic nontransgenic donors. The resultant liver disease, hepatocyte apoptosis, regeneration, and tumor development were assessed and compared with the manifestations in mice that had received unfractionated spleen cells. Transfer of $CD8^+$-enriched splenocytes caused prolonged disease kinetics, and a marked increase in the extent of hepatocyte apoptosis and regeneration. In 12 of 14 mice the transfer resulted in multiple hepatocellular carcinomas (HCCs) comparable with the manifestations seen in the mice transferred with total splenocytes. In contrast, mice that had received $CD4^+$-enriched cells demonstrated lower levels of liver disease and developed fewer incidences of HCC (4 of 17). The experiment also revealed that all of the groups of mice complicated with HCC developed comparable mean numbers and sizes of tumors. B-cell depletion had no effect on disease kinetics in this model. Taken together, these results demonstrate that the pathogenetic events induced by $CD8^+$ T-cell subset are primarily responsible for the induction of chronic liver disease that increases tumor incidence, suggesting their potential in triggering the process of hepatocarcinogenesis.

INTRODUCTION

Hepatocellular carcinoma (HCC) occurs after many years of chronic hepatitis (1, 2). During the process, both viral and host factors have been implicated in liver cell transformation and carcinogenesis. On the one hand, some viral proteins, *i.e.*, hepatitis B virus (HBV) X protein (3, 4) and hepatitis C virus core protein (5, 6), are considered to contribute to tumor development in the liver, because high-level expression of the proteins increases the incidence of HCC in transgenic mice. Furthermore, most tumors contain clonally integrated HBV DNA and microdeletions in the flanking cellular DNA, which could theoretically deregulate cellular growth control mechanisms (7). And COOH-terminally truncated viral envelop proteins expressed from integrated subviral DNA may have transactivating activity (8, 9) and could potentially contribute to carcinogenesis in chronic HBV infection.

On the other hand, prolonged inflammation is thought to set up a cycle of liver cell destruction and regeneration, resulting in a mitogenic and mutagenic environment that can precipitate random genetic and chromosomal damage, and lead to the development of HCC (10–12). In patients with chronic hepatitis B and C, $CD4^+$ and $CD8^+$ T lymphocytes specific for the viruses are detectable in the peripheral blood and in intrahepatic infiltrates, and are suggested to play a role in the immune pathogenesis of liver disease (13–16). Furthermore, transfer of the virus-specific $CD4^+$ and $CD8^+$ T-cell clones was observed to induce acute necroinflammatory liver disease in the models of HBV transgenic mice (17–20). However, the relative contribution of $CD4^+$ and $CD8^+$ T lymphocytes to the induction of chronic liver cell injury was not determined, because the T-cell clones induced neither prolonged liver diseases nor HCC in the models of acute hepatocellular injury, and because the animal model that pathophysiologically reproduces human chronic viral hepatitis was not available. In an effort to clarify the carcinogenic potential of chronic inflammation, we have developed a model of chronic immune-mediated liver disease using HBV transgenic mice that express the envelop proteins in the hepatocytes (21). The results demonstrate that continuous intrahepatic inflammation is sufficient to cause liver cancer in the absence of pre-existing viral transactivation, insertional mutagenesis, or genotoxic chemicals during chronic HBV infection.

We have shown recently that the administration of anti-Fas ligand (FasL) neutralizing antibody reduces hepatocyte apoptosis, proliferation, and liver inflammation, and eventually diminishes the development of HCC. This observation suggests a critical involvement of FasL-induced pathogenetic events in the process of hepatocarcinogenesis (22). We have also reported evidence that the FasL-dependent pathway is critically involved in the development of acute liver cell injury induced by $CD8^+$ cytotoxic T-lymphocyte (CTL) clones (23, 24). Because FasL is known to be expressed on activated T lymphocytes (25–29), we speculated that the $CD8^+$ T-cell subset was implicated as a causative factor responsible for the chronic liver cell injury that promotes hepatocarcinogenesis.

To determine the involvement of immune cell subsets in the progression of chronic liver disease, the current experiment was performed in the model of chronic immune-mediated hepatitis in which T- and B-cell subset-depleted or -enriched splenocytes obtained from HBV-primed, nontransgenic mice were transferred into the transgenic recipients, and liver disease and tumor development were monitored. The results demonstrate that each cell subset causes unique kinetics of liver disease and different incidence of liver cancer.

MATERIALS AND METHODS

HBV Transgenic Mice. Hepatitis B surface antigen (HBsAg) transgenic mouse lineage 107–5D [official designation Tg(Alb-1, HBV)Bri66; inbred B10D2, H-2^d] was kindly provided by Dr. Francis V. Chisari (The Scripps Research Institute, La Jolla, CA; Ref. 30). Lineage 107–5D contains the entire HBV envelope coding region (subtype ayw) under the constitutive transcriptional control of the mouse albumin promoter (30). These mice express the HBV small, middle, and large envelope proteins in their hepatocytes (30, 31), they are immunologically tolerant to HBsAg at the T-cell level (32), and they display no evidence of liver disease during their lifetime although they do develop "ground glass" hepatocytes due to overexpression of the large envelope protein (30). There is no X-RNA or X-protein expression detectable in the livers of these animals.[4] Importantly, the mice develop a severe MHC class I-restricted necroinflammatory liver disease after the adoptive transfer of HBsAg-specific CTLs (17, 18, 30).

Received 12/6/03; revised 2/5/04; accepted 2/25/04.

The costs of publication of this article were defrayed in part by the payment of page charges. This article must therefore be hereby marked *advertisement* in accordance with 18 U.S.C. Section 1734 solely to indicate this fact.

Requests for reprints: Shuichi Kaneko, Department of Gastroenterology; Graduate School of Medicine, Kanazawa University; 13-1 Takara-machi, Kanazawa 920-8641, Japan. Phone: 81-76-265-2231; Fax: 81-76-234-4250; E-mail: skaneko@medf.m.kanazawa-u.ac.jp.

[4] Unpublished observations.

Disease Model. To break tolerance at the B- and T-cell levels, HBV transgenic mice were thymectomized, bone marrow-reconstituted, and adoptively transferred with nontransgenic immune systems according to the procedures described previously (21, 33). Briefly, 8–10-week-old male transgenic mice were thymectomized. Seven days later the mice were irradiated (900 cGy) and then reconstituted by the i.v. injection of 10^7 bone marrow cells collected from the femurs and tibias of syngeneic nontransgenic B10D2 (H-2^d) mice. One week after the bone marrow transfer, the animals were injected i.v. with the indicated numbers of splenocyte subsets from nontransgenic B10D2 (H-2^d) mice that were infected i.p. with a recombinant vaccinia virus expressing HBsAg (HBs-vac) 3 weeks before the splenocyte transfer (17). At the same time, transfer of total splenocytes from the primed nontransgenic mice and the unprimed transgenic littermates were performed for control purposes. The resultant hepatocellular injury was monitored biochemically as serum alanine aminotransferase (ALT) activity (10). Results were expressed as mean units per liter ± SE of serum ALT activity, and differences between groups were assessed for statistical significance by Student's *t* test. Tumor development was assessed by abdominal palpation and confirmed by autopsy at which time the number of tumors visible at the surface of each liver was counted, and the diameter of each tumor was measured with a millimeter rule. All of the experiments satisfied the Guidelines for the Care and Use of Laboratory Animals in Takara-machi Campus of Kanazawa University.

Depletion and Enrichment of T- and B-Cell Subsets. To deplete $CD4^+$ or $CD8^+$ T cells, splenocytes were treated with monoclonal antibodies (mAbs) specific for CD4 (GK1.5) or CD8 (2.43; American Type Culture Collection, Manassas, VA), respectively, and then with rabbit complement (Cedarlane, Hornby, Ontario, Canada). B cells of splenocytes were depleted on the Mouse T Cell immunocolumn (Cytovax, Edmonton, Alberta, Canada), by treatment with mAb specific for MHC class II I-A^d (MK-D6; American Type Culture Collection), and with rabbit complement. To enrich $CD4^+$ or $CD8^+$ T cells, splenocytes were passed over the Mouse T Cell immunocolumn and treated with a combination of anti-CD8 and anti-I-A^d mAbs, or anti-CD4 and anti-I-A^d mAbs, respectively, and then with rabbit complement. The purity of the T- and B-cell populations was monitored by immunolabeling with FITC-conjugated rat mAb specific for mouse CD4 (RM4–5; BD PharMingen, San Diego, CA), and phycoerythrin-conjugated rat mAb specific for mouse CD8 (53–6.7), or CD19, which is a B cell-specific transmembrane protein (1D3; BD PharMingen), followed by fluorescence-activated cell sorter analysis.

Immunohistochemical Analysis. Tissue samples were fixed in buffered zinc formalin (Anatech Ltd., Battle Creek, MI), embedded in paraffin, sectioned (at 3 μ m), and stained with H&E as described previously (21). Some of the paraffin sections were treated with anti-proliferating cell nuclear antigen (PCNA) and anti-HBsAg primary solutions (Dako, Carpinteria, CA) at 1:10 and 1:1000 dilutions, respectively, followed by biotin-conjugated secondary antibody (Vector Laboratories, Inc., Burlingame, CA; Ref. 34). $PCNA^+$ and $HBsAg^+$ cells were then visualized using a VECTASTAIN ABC Standard kit (Vector Laboratories), and the tissue sections were counterstained with hematoxylin before mounting. Liver tissue samples were also embedded in OCT compound (Sakura Finetek, Torrance, CA) and snap-frozen in liquid nitrogen. Cryostat sections of frozen tissues were fixed in 4% paraformaldehyde overnight at 4°C. After blocking biotin, the tissue sections were incubated with rabbit antimouse active caspase-3 antibodies (35) at a 1:400 dilution for 30 min at room temperature, followed by biotin-conjugated goat antirabbit IgG secondary antibodies (Vector Laboratories). The reaction was visualized in the same way as the PCNA staining described above. Terminal deoxynucleotidyl transferase-mediated nick end labeling (TUNEL) analysis was performed on serial liver sections according to the manufacturer's instructions (Roche, Indianapolis, IN).

RESULTS

Cellular Basis for Prolonged Chronic Immune-Mediated Hepatitis in HBV Transgenic Mice. To determine the relative contribution of immune cell subsets to prolonged chronic immune-mediated hepatitis in HBV transgenic mice, the splenocytes isolated from HBsAg-primed nontransgenic mice were depleted (Fig. 1) or enriched (Fig. 2) of $CD4^+$ and $CD8^+$ T cells and $CD19^+$ B cells, and they were then adoptively transferred into thymectomized, bone marrow-reconstituted HBV transgenic recipients. The kinetics of all of the disease manifestations was compared with that caused by total splenocyte transfer. As observed previously (21), total cell transfer caused prolonged chronic hepatitis (Fig. 1). Briefly, serum ALT activity increased from preinjection levels of 20–40 units/liter to approximately 2000–4000 units/liter within 7 days after adoptive transfer and fell progressively thereafter. Importantly, the ALT activity never returned to baseline in these animals, remaining at least two to three times above normal throughout the experiment. B cell-depleted splenocytes demonstrated disease kinetics comparable with that seen after total cell transfer. Similarly, $CD4^+$ subset-depleted splenocytes caused acute elevation of serum ALT activity within 7 days after the transfer, and the animals developed persistent liver disease, although the peak of disease activity was lower than that seen after total cell transfer. In contrast, $CD8^+$ subset depletion markedly reduced the peak and diminished the disease activity in the chronic phase later than 7 days. In addition, we assume that a contaminating 1.4% (1.3×10^6) of $CD8^+$ T cells in this $CD8^+$ subset-depleted population may not influence the kinetics of liver disease, because we observed that transfer of 1×10^7 total splenocytes, which contained ~20% (2×10^6) $CD8^+$ T cells, did not cause elevation of ALT in this model.[4]

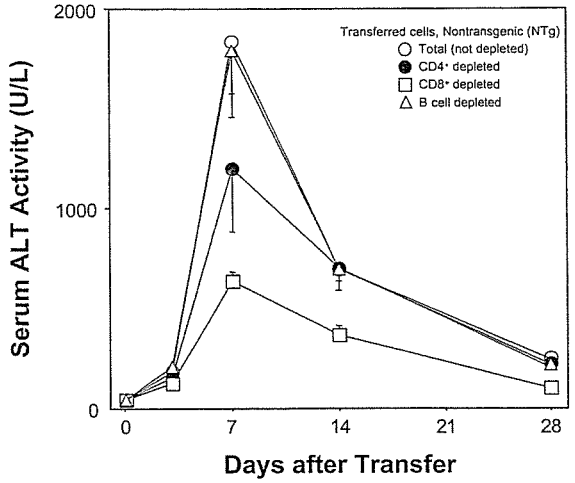

Fig. 1. Kinetics of serum alanine aminotransferase (*ALT*) after transfer of $CD4^+$ T cell-depleted, $CD8^+$ T cell-depleted, or B cell-depleted splenocytes in a transgenic mouse model of chronic hepatitis B. The splenocytes were obtained from hepatitis B surface antigen-primed, syngeneic nontransgenic mice. Nine $\times$ 10^7 cells of the splenocytes depleted of $CD4^+$, [$CD4^+$, 1.4%; $CD8^+$, 20.8%; B ($CD19^+$), 32.4%], $CD8^+$ ($CD4^+$, 15.0%; $CD8^+$, 1.4%; B, 28.5%), or B cells ($CD4^+$, 17.5%; $CD8^+$, 38.5%; B, 0.1%) were transferred into hepatitis B virus transgenic mice. At the same time, transfer of the total splenocytes (1×10^8 cells; $CD4^+$, 12.7%; $CD8^+$, 16.7%; B, 26.8%) was performed for control purposes. The serum ALT activity (mean units/liter) was monitored to evaluate liver injury; *bars*, ±SE. Each group represents 5 animals.

Consistent with the differences in the kinetics of liver disease induced by the subset-depleted cells, transfer of $CD8^+$ subset-enriched splenocytes displayed the prolonged kinetics comparable with total cell transfer except for the lower peak of ALT (Fig. 2). In contrast, $CD4^+$ subset-enriched cells caused a transient elevation of ALT 7 days after adoptive transfer that seemed to improve 14 days after the transfer. In addition, we confirmed that transgenic splenocytes induce no disease in the recipient mice, indicating that all subsets of transgenic splenocytes are perfectly immunologically tolerant to the viral antigens as observed previously (21). Whereas these subset-enriched splenocytes included unidentified non-T and non-B cells that might influence the kinetics of liver disease, the data collectively demonstrate that $CD8^+$ T lymphocytes contributed not

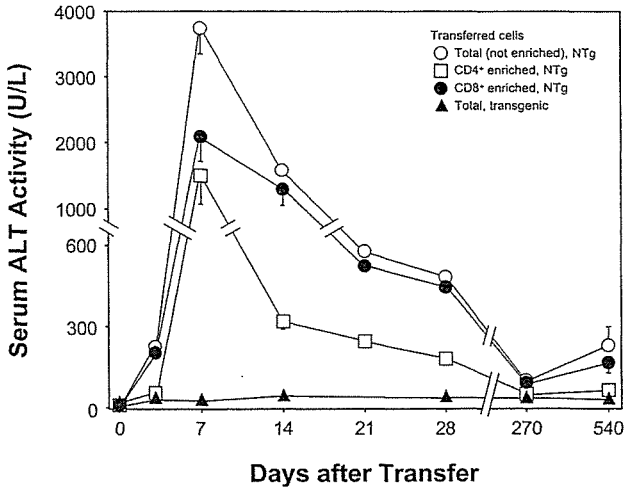

Fig. 2. Kinetics of serum alanine aminotransferase (*ALT*) after transfer of $CD4^+$ or $CD8^+$ T cell-enriched splenocytes in a transgenic mouse model of chronic hepatitis B. The splenocytes were obtained from hepatitis B surface antigen-primed, syngeneic nontransgenic mice. Five × 10^7 cells of the splenocytes enriched for $CD4^+$ ($CD4^+$, 78.7%; $CD8^+$, 1.8%; B, 0.9%) or $CD8^+$ ($CD4^+$, 2.0%; $CD8^+$, 84.2%; B, 0.7%) were transfused into hepatitis B virus transgenic mice. At the same time, transfer of total splenocytes from the primed nontransgenic mice (1 × 10^8 cells; $CD4^+$, 10.4%; $CD8^+$, 21.3%; B, 23.0%) and the unprimed transgenic littermates (1 × 10^8 cells) were performed for control purposes. The serum ALT activity (mean units/liter) was monitored to evaluate liver injury; *bars*, ±SE. Each group represents 5 animals. Similar experiments were performed three times and representative data are shown.

only to the induction of hepatocellular injury but also to the maintenance of disease activity in the HBV transgenic mouse model.

In the analysis of liver histology (Fig. 3, *A* and *B*) the mice transferred with total splenocytes and with $CD8^+$ subset-enriched cells demonstrated severe infiltration of inflammatory cells, apoptotic and necrotic hepatocytes, many necroinflammatory foci, and mitotic figures. In contrast, the liver samples of mice transferred with the $CD4^+$ subset-enriched cells showed reduced infiltration of inflammatory cells, and minimal induction of apoptosis and liver cell injury. Consistent with the differences in disease activity revealed by the change in the serum ALT level, the results indicate that the $CD8^+$ subset was critically involved in the histological changes of pathological features associated with the establishment of prolonged chronic hepatitis seen in this model.

Apoptosis and Regeneration of Hepatocytes Induced by Differential Immune Cell Subsets in Prolonged Chronic Liver Disease. To monitor the hepatocyte destruction and regeneration caused by inflammation with immune cell subsets, the activation of the caspase cascade was determined immunohistochemically using mAb specific for the activated form of caspase-3. Degradation of DNA from apoptotic hepatocytes was measured by nuclear staining using the TUNEL method, and hepatocyte proliferation was assessed with mAb specific for PCNA (Fig. 4, *A* and *B*). Consistent with the differences in the serum levels of ALT activity, $CD8^+$ subset-enriched splenocytes induced marked caspase-3 activation and DNA degradation, comparable with the effects seen with total splenocytes, whereas CD4 enrichment diminished the number of active caspase-3^+ and $TUNEL^+$ hepatocytes. A pair of serial sections in mirror-image orientation stained with antiactive caspase-3 antibodies and the TUNEL method revealed that strong caspase-3 activation and DNA degradation were occurring in hepatocytes along the edge of the area where massive infiltrating cells were found. These data suggest that massive hepatocyte apoptosis may be caused by extensive infiltration of the transferred $CD8^+$ splenocyte subset into the liver tissues. In addition, the observation at the single cell level indicated that the hepatocytes stained by the antiactive caspase-3 and by the TUNEL method did not seem to perfectly coincide. We speculate that this could be due to the difference in the phase of apoptotic process, because caspase activation and DNA degradation may be detected in the earlier and the later phases by the two independent methods, respectively.

We also observed many $PCNA^+$ hepatocytes when total and $CD8^+$ subset-enriched splenocytes were transferred. In contrast, we found only a few $PCNA^+$ hepatocytes in mice transfused with $CD4^+$ cells, where most of the $PCNA^+$ cells were infiltrating inflammatory cells. Taken together, these results indicate that $CD8^+$ T cells played a major role in induction of hepatocyte apoptosis and regenerative hepatocyte proliferation in this hepatitis model; $CD4^+$ T cells did, however, play a minor role, especially in an early period of the acute phase.

Hepatocarcinogenesis Associated with Prolonged Chronic Liver Disease Induced by Differential Immune Cell Subsets. We have reported that HCC development was primarily dependent on prolonged chronic inflammation in the liver after transfer of HBsAg-primed, total splenocytes (21). To evaluate the relative procarcinogenic potential of liver disease induced by differential immune cell subsets, tumor development was monitored for 11–22 months in the mice transferred with the primed splenocyte subsets (Table 1). Twelve of the 14 animals transferred with $CD8^+$ subset-enriched splenocytes developed HCC, the incidence of which was comparable with that seen after total cell transfer (11 of 12; Refs. 21, 22). Most of them displayed multiple tumors, the size of the largest tumor was ranging up to 20 mm in diameter, and they illustrated the classical histological features of well-differentiated HCC including clear cells (Fig. 5, *A* and *F*). The surrounding hepatic parenchyma displayed focal lobular inflammatory infiltrates associated with degenerating hepatocytes, marked lobular disarray, fatty deposits, and clear tumor cell nests. The expression of HBsAg was abolished or decreased to a great extent in the tumor cells probably due to the altered transcription state (10, 11), whereas it was detectable in the surrounding parenchyma (Fig. 5, *B* and *G*). Even in the surrounding tissue the levels of expression were diminished, which was presumably due to long-term persistent inflammatory stimulation via noncytolytic cytokine-dependent mechanisms (36, 37). In addition, well-differentiated HCC consisting of tumor cells with large amounts of fatty deposits (Fig. 5*C*) were seen in the same liver tissue of the mouse indicated in Fig. 5*A*, suggesting a high potential for tumorigenesis induced by chronic immune-mediated liver disease. In tumor tissues of the mice transferred with $CD8^+$ subset-enriched cells, we observed both highly differentiated, fat deposited neoplastic hepatocytes (Fig. 5*H, right area*) and poorly differentiated, sarcomatous components (Fig. 5*H, left area*). Furthermore, 2 of the mice were complicated with the rupture of HCC and bloody ascites (Fig. 5, *I* and *J*). All of the data indicate that prolonged chronic inflammation caused by the $CD8^+$ subset displayed virtually the same effects as that by total splenocytes on the induction of hepatocarcinogenesis.

In contrast, the animals transferred with $CD4^+$ subset-enriched splenocytes displayed a lower potential for hepatocarcinogenesis, in which 4 of the 17 mice developed HCC (Table 1). However, the tumors were histologically identical to those in the animals transferred with total splenocytes (Fig. 5, *D* and *E*). Interestingly, the numbers and sizes of tumors were comparable among the mice complicated with HCC after the transfer with total, $CD4^+$, or $CD8^+$ subset-enriched splenocytes [numbers of liver tumors/sizes (mm) in diameter of largest tumors (means ± SE); 4.2 ± 2.1/8.9 ± 1.7, 3.3 ± 1.3/7.8 ± 2.4, and 3.0 ± 0.7/10.2 ± 1.0, respectively; $P > 0.5$] (Table 1). The data indicate that the pathogenetic events induced by individual

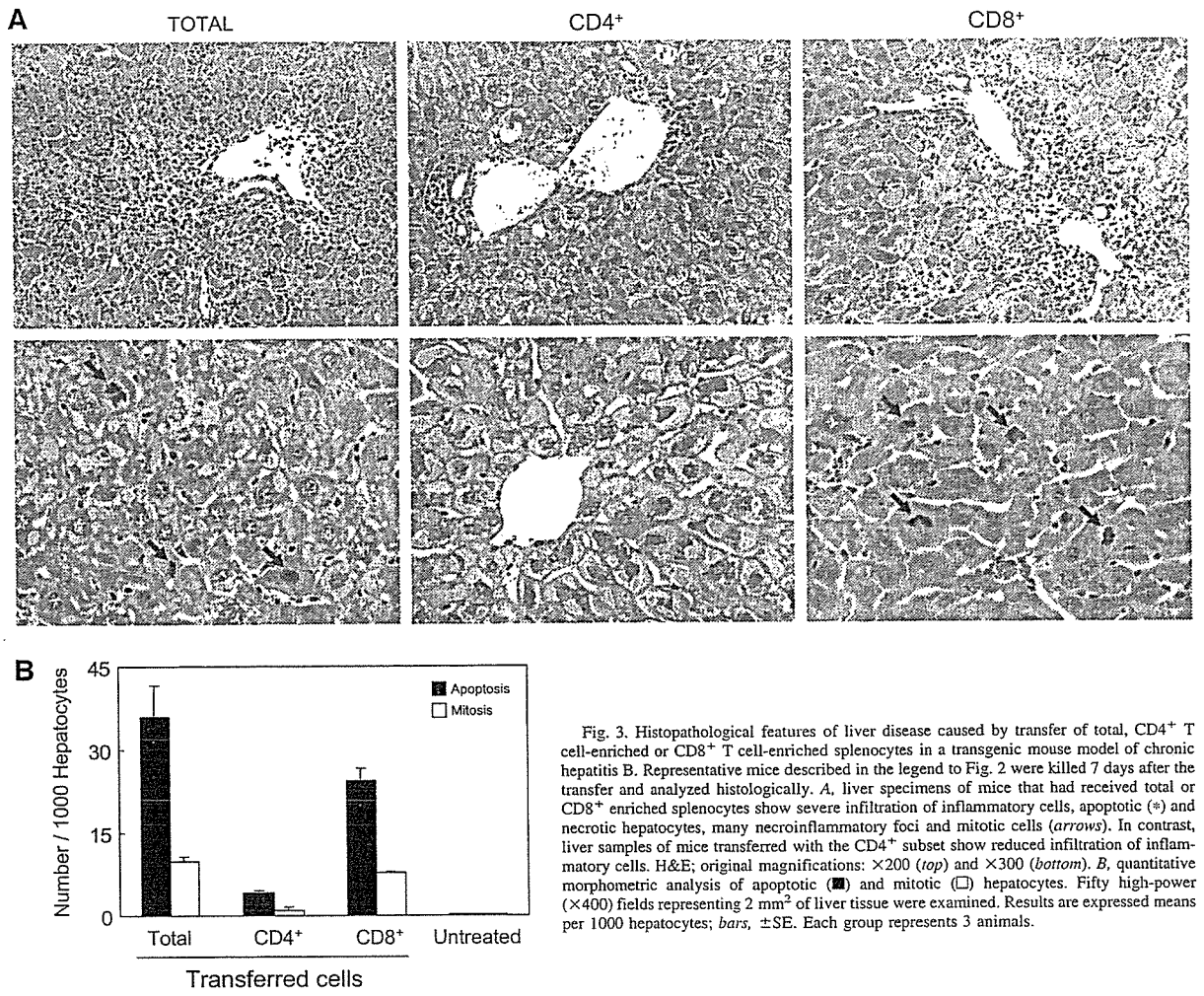

Fig. 3. Histopathological features of liver disease caused by transfer of total, $CD4^+$ T cell-enriched or $CD8^+$ T cell-enriched splenocytes in a transgenic mouse model of chronic hepatitis B. Representative mice described in the legend to Fig. 2 were killed 7 days after the transfer and analyzed histologically. *A*, liver specimens of mice that had received total or $CD8^+$ enriched splenocytes show severe infiltration of inflammatory cells, apoptotic (*) and necrotic hepatocytes, many necroinflammatory foci and mitotic cells (*arrows*). In contrast, liver samples of mice transferred with the $CD4^+$ subset show reduced infiltration of inflammatory cells. H&E; original magnifications: ×200 (*top*) and ×300 (*bottom*). *B*, quantitative morphometric analysis of apoptotic (■) and mitotic (□) hepatocytes. Fifty high-power (×400) fields representing 2 mm^2 of liver tissue were examined. Results are expressed means per 1000 hepatocytes; *bars*, ±SE. Each group represents 3 animals.

T-cell subsets influenced the potential in triggering the process of hepatocarcinogenesis rather than promoting tumor growth thereafter, resulting in different incidence of liver tumor. In addition, the mice thymectomized, irradiated, and transferred with splenocytes from the syngeneic transgenic animals or the unmanipulated controls developed no liver tumors. Collectively, the results demonstrate that each subset of the immune cells may individually contribute to the HCC development in this model. The $CD8^+$ subset plays a primary role in the maintenance of chronic liver disease and induction of liver tumors, whereas the $CD4^+$ subset displays a minimal potential for tumorigenesis during the process of prolonged chronic inflammation in the liver.

DISCUSSION

The current study indicates that T cells, especially the $CD8^+$ subset, rather than B cells are primarily responsible for the induction of prolonged liver injury in a mouse model of viral hepatitis. In contrast to the $CD8^+$ T-cell subset, $CD4^+$ T cells caused milder hepatic injury that seemed to improve shortly after the transfer as seen at the transaminase level. Consistent with the severity and duration of persistent liver disease, $CD8^+$ T cells displayed strong induction of hepatocellular apoptosis, inflammation, and regenerative proliferation that sets up a cycle of liver cell destruction and regeneration. Furthermore, the pathogenetic events induced by individual T-cell subsets exerted their different potential in triggering the oncogenic process of hepatocarcinogenesis. On the basis of these results, we suggest that $CD8^+$ T lymphocytes can principally contribute to the progression of chronic liver disease and the initiation of a complex sequence of events that leads to the development of HCC.

In the previous study, we observed that $CD8^+$ CTL clones caused liver cell apoptosis by activating the FasL/Fas-, perforin/granzyme-, and cytokine-dependent death pathways in the model of acute hepatocellular injury (24). Additionally, the liver cell injury was amplified by inflammation that may be exaggerated by FasL expressed on $CD8^+$ CTL clones (18, 19). Similarly, the histological findings in the current study indicated that an intracellular caspase cascade, which is a death pathway of hepatocytes, was strongly activated after $CD8^+$ T-cell transfer, and hepatocyte apoptosis was detectable along the area with inflammatory infiltrates. The massive cell loss through inflammation was thought to stimulate the regenerative proliferation of hepatocytes. These data suggest that the effector mechanism for chronic liver disease induced by $CD8^+$ T cells may be similar to acute liver cell injury induced by the CTL clones.

In other mouse models, liver cell injury was induced by transfer of $CD8^+$ CTL clones or hepatotoxic agents, and demonstrated

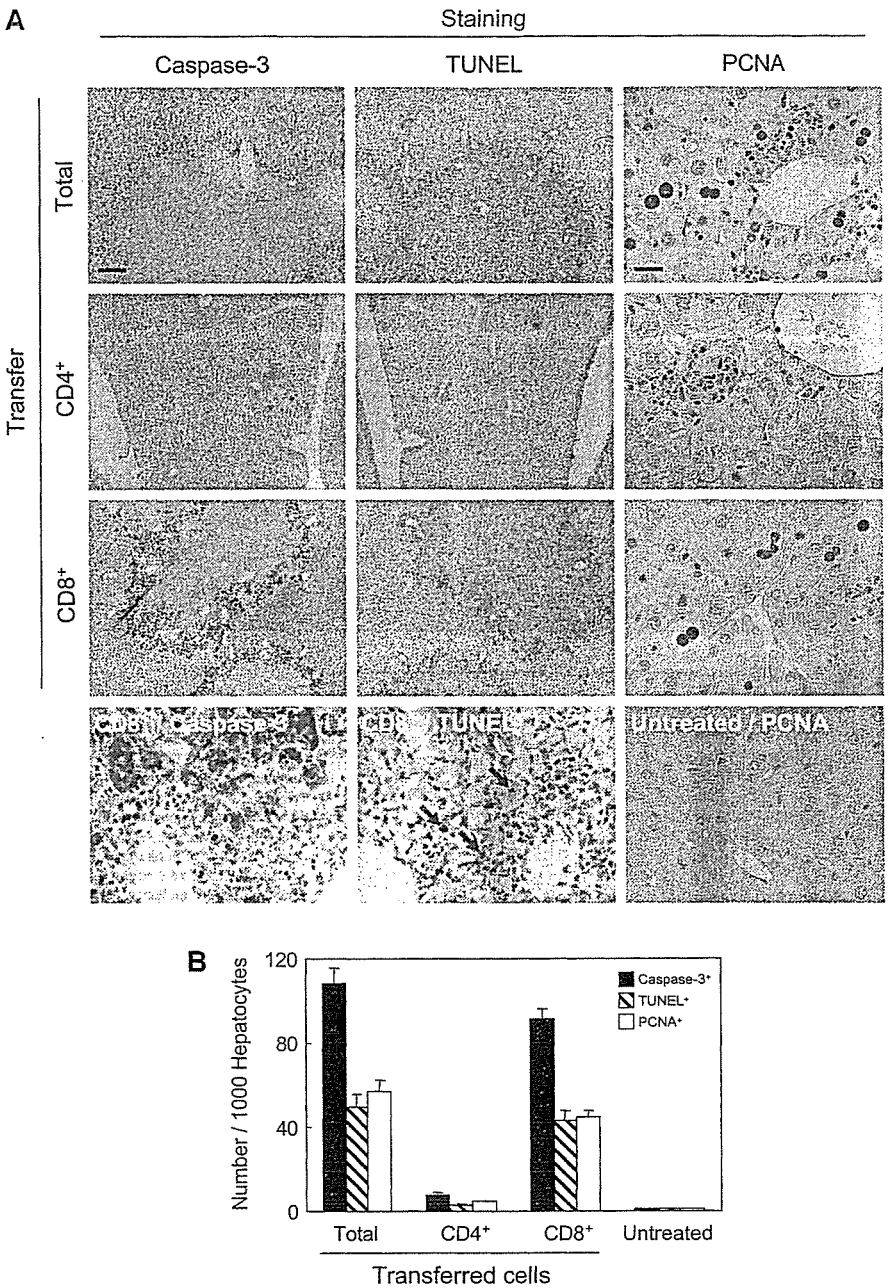

Fig. 4. Immunohistochemical analysis of hepatocellular apoptosis and regeneration induced by transfer of total, $CD4^+$ T cell-enriched or $CD8^+$ T cell-enriched, splenocytes in a transgenic mouse model of chronic hepatitis B. Representative mice described in the legend to Fig. 2 were killed 7 days after the transfer. *A*, immunohistochemical analysis of active caspase-3 and terminal deoxynucleotidyl transferase-mediated nick end labeling (TUNEL) analysis were performed in mirror-image serial sections of the liver tissues. $TUNEL^+$ hepatocyte nuclei are indicated with *arrows* . Proliferating cell nuclear antigen (PCNA) expression was analyzed in the same tissues. Age-matched, untreated hepatitis B virus transgenic mouse liver was stained for PCNA as a control. Original magnifications, ×40 (*top three panels* of caspase-3 and TUNEL staining; *bar* represents 200 μ m), and ×400 (the *other panels*: *bar* represents 20 μm). *B*, quantitative morphometric analysis of caspase-3^+ (■), $TUNEL^+$ (▨) and $PCNA^+$ (□) hepatocytes. Fifty high-power (×400) fields representing 2 mm^2 of liver tissue were examined. Results are expressed means per 1000 hepatocytes; *bars*, ±SE. Each group represents 3 animals.

acute, self-limited kinetics (17, 18, 30, 38). In the current experiment, prolonged immune-mediated hepatitis was established after transfer of $CD8^+$ T cells obtained from HBsAg-primed, nontransgenic mice to the transgenic recipients. We speculated that the transferred, $CD8^+$ T cells primarily contributed to the unique kinetics of liver disease because the $CD8^+$ subset of splenocytes were prepared without an *in vitro* stimulation, indicating that not only effector but also memory T cells were included in the transplanted cells. $CD8^+$ memory T cells were reported recently to have a longer life span than $CD4^+$ memory T cells (39). Thus, the lymphocytic choriomeningitis virus-specific $CD8^+$ T cells appeared to survive in secondary lymphoid organs (periphery) and display their antiviral effects for >2 years (40–42). Consistent with this finding, we observed previously that the HBsAg-specific, $CD8^+$ CTL response was detected in the splenocytes 17 months after adoptive transfer in this chronic disease model (21). Collectively, the transferred, memory $CD8^+$ T cells are estimated to home to and survive in secondary lymphoid organs for >1 and 1.5 years, and suggested to continuously supply effector T cells into liver tissue through blood flow, which can recognize HBsAg expressed on the hepatocytes and maintain hepatocellular injury.

During the carcinogenetic process, it has been suggested that latent genetic mutations in the cells can be induced to undergo clonal selection in the initiation stage, and that the growth of the initiated cells that carry the first mutation can be stimulated in the promotion stage (43). Accordingly, the oncogenic potential in the initiation and

Table 1 *Hepatocarcinogenesis after transfer of differential immune cell subsets*

Mouse ID	Months after spl.[a] transfer	Age (mo.) at killing	No. of tumors	Largest tumor (mm)[b]	Tumor histology
Transferred with total, HBsAg-primed nontransgenic splenocytes (1×10^8 cells; $CD4^+$, 10.4%; $CD8^+$, 21.3%; B, 23.0%)					
46	22	24	1	10	HCC
56	16	19	3	10	HCC
60	18	21	2	20	HCC
85	18	21	3	3	HCC
88	17	20	1	4	HCC
131	17	19	2	8	HCC
185	11	14	3	3	HCC
198	15	18	1	3	Adenoma
227	13	16	1	5	HCC
269	15	18	>25[c]	15	HCC
265	15	18	4	5	HCC
280	21	23	1	15	HCC
Mean (range)	16.5 (11–22)	19.3 (14–24)	3.9 (1–25<)	8.4 (3–20)	
Transferred with $CD4^+$ T cell-enriched, HBsAg-primed nontransgenic splenocytes (5×10^7 cells; $CD4^+$, 78.7%; $CD8^+$, 1.8%; B, 0.9%)					
98	16	19	0	0	
99	17	20	2	6	HCC
137	15	17	0	0	
172	19	22	0	0	
201	15	18	0	0	
202	12	15	0	0	
211	17	19	2	2	Adenoma
248	14	17	0	0	
275	22	25	3	15	HCC
276	15	18	0	0	
304	18	21	1	5	HCC
305	18	21	7	5	HCC
307	18	21	0	0	
308	18	21	0	0	
322	18	20	0	0	
323	18	20	0	0	
327	18	20	1	3	Adenoma
Mean (range)	16.9 (12–22)	19.6 (15–25)	0.9 (0–7)	2.1 (0–15)	
Transferred with $CD8^+$ T cell-enriched, HBsAg-primed nontransgenic splenocytes (5×10^7 cells; $CD4^+$, 2.0%; $CD8^+$, 84.2%; B, 0.7%)					
91	17	20	1	10	HCC
132	18	20	8	15	HCC
209	18	21	3	8	HCC
224	12	15	3	5	HCC
225	16	19	1	7	HCC
283	14	16	1	17	HCC
313	18	21	2	10	HCC
314	16	19	5	10	HCC
316	18	21	6	7	HCC
296	16	19	1	9	HCC
334	18	20	0	0	
335	18	20	1	14	HCC
338	18	20	4	10	HCC
298	18	21	1	3	Adenoma
Mean (range)	16.8 (12–18)	19.4 (15–21)	2.6 (0–8)	8.9 (0–17)	
Transferred with total (1×10^8 cells; $CD4^+$, 17.5%; $CD8^+$, 11.7%; B, 25.8%)					
142[d]	19	22	0	0	
147[d]	19	22	0	0	
152[d]	15	18	0	0	
161[d]	12	15	0	0	
9[e]	0	17	0	0	
220[e]	0	17	0	0	
221[e]	0	18	0	0	
233[e]	0	19	0	0	
254[e]	0	20	0	0	
368[e]	0	20	0	0	
369[e]	0	21	0	0	
235[e]	0	22	0	0	
236[e]	0	22	0	0	
238[e]	0	23	0	0	
288[e]	0	24	0	0	
Mean (range)	ND	20.0 (15–24)	0	0	

[a] spl., splenocyte; HBsAg, hepatitis B surface antigen; ND, not determined; HCC, hepatocellular carcinoma.
[b] Diameter in the major axis.
[c] Attributed to 25 for statistical analysis.
[d] Immunologically tolerant transgenic splenocytes.
[e] Unmanipulated.

the promotion stages may be reflected by the numbers and sizes of tumors, respectively. In the current study, the transfer of the $CD4^+$ and $CD8^+$ T-cell subsets caused differences not in the numbers or sizes but in the incidences of HCC, suggesting that the pathogenetic events directly affected neither stage of carcinogenesis. We speculate that the events induced by the individual subsets might be involved in triggering carcinogenetic environment to different extents in the earlier stage than in the initiation. And, irrespective of the causative T-cell subsets, initiation and promotion of HCC would occur when such environment was generated. This sequence of events suggests that the regulation of T cell-induced environment in the early period of hepatocarcinogenesis may inhibit tumor cell initiation and cancel

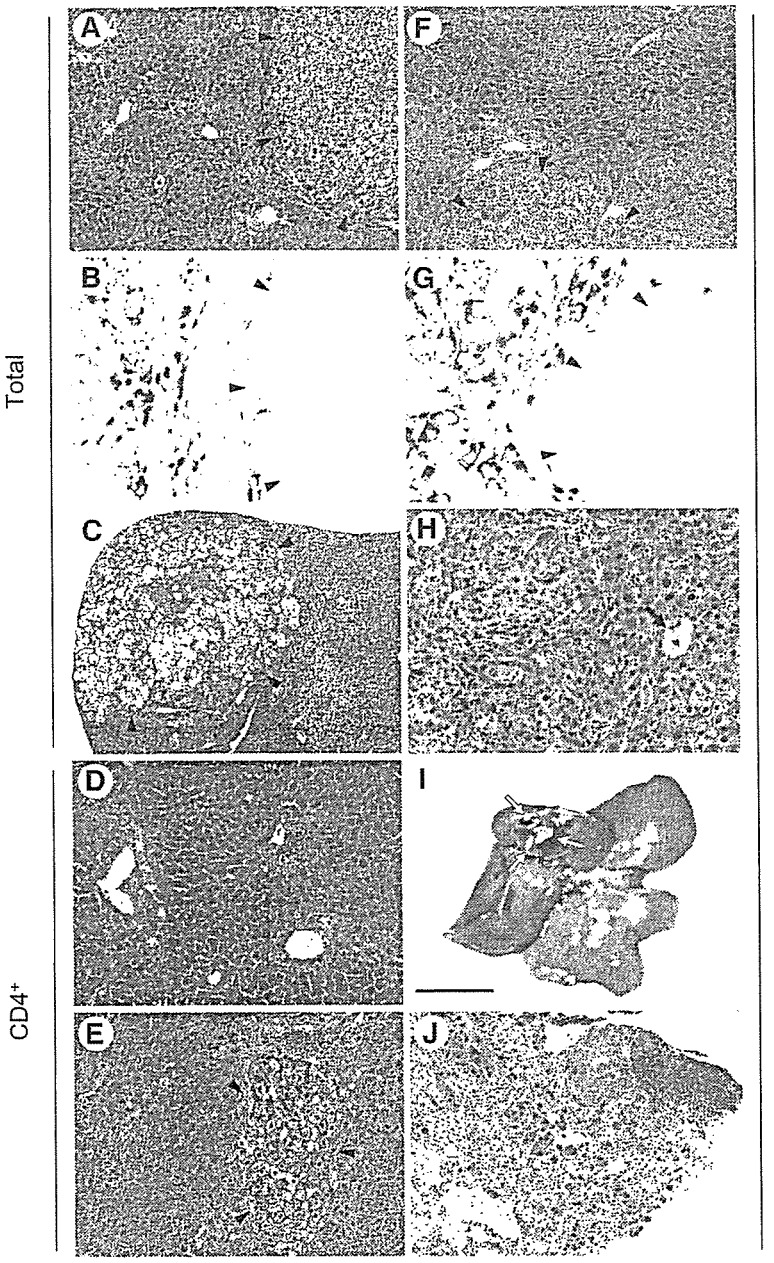

Fig. 5. Histopathological features of progressive liver disease and hepatocellular carcinomas (HCC) development after transfer of total (*A–C*), $CD4^+$ T cell-enriched (*D* and *E*) or $CD8^+$ T cell-enriched (*F–J*) splenocytes in a transgenic mouse model of chronic hepatitis B. The mice described in the legend to Fig. 2 were killed >11 months after the transfer, and liver tissues were stained with H&E (*A, C–F, H,* and *J*) and for hepatitis B surface antigen (HBsAg; *B* and *G*). Tumors in mice transferred with total splenocytes display histological evidence of well-differentiated HCC (*arrowheads; A*). The surrounding hepatic parenchyma show focal lobular inflammatory infiltrates associated with degenerating hepatocytes and marked lobular disarray. HBsAg expression is abolished in the tumor cells (*arrowheads*), whereas it is detectable in the surrounding parenchyma (*B*). In the same liver tissue as in *A*, well-differentiated HCC is seen that consists of tumor cells with large amounts of fatty deposits (*arrowheads; C*). Animals that received $CD4^+$-enriched cells demonstrate lower levels of inflammatory infiltrates (*D*) and clear tumor cell nests (*arrowheads; E*). Comparable with the mice that received total splenocyte transfer, animals that received $CD8^+$-enriched cells show well-differentiated HCC including clear cells (*arrowheads; F*), the histological features of chronic liver disease in the surrounding hepatic parenchyma, and the suppression of HBsAg expression in the tumor cells (*arrowheads; G*). In tumor tissues, both highly differentiated, fat-deposited neoplastic hepatocytes (*arrow; H, right area*) and sarcomatous component (*H, left area*) were seen. Furthermore, the mice were complicated with the rupture of HCC (*arrows; I* and *J*). Original magnifications: ×100 (*A, D, E, F,* and *J*), ×40 (*C*), and ×200 (*B, G,* and *H*). The *bar* represents 10 mm (*I*).

the following malignant transformation leading to tumor development.

The precise mechanisms of hepatocarcinogenesis during chronic viral hepatitis still remain unanswered. Within the entire spectrum of carcinogenic pathways including hepatic cell injury (13, 44, 45), proliferation (46–48), altered gene expression (49, 50), and the role of p53 (51–54), the current study design evaluating the late events in the carcinogenic process may not be sufficient to discuss the disease hypothesis. However, it is most likely, based on the striking similarity of the disease processes in human viral hepatitis and the animal model used in the current study (21, 22), that the T-cell subsets are critically involved in the pathogenesis of HCC associated with chronic hepatitis B. Elucidating the contribution of immunological events to the HCC development should be important not only for understanding the pathogenesis of liver cancer, but also for establishing new cancer-preventive treatments for patients with viral hepatitis.

ACKNOWLEDGMENTS

We thank Dr. Francis V. Chisari for kindly providing us the HBsAg transgenic mice, and Akemi Nakano, Yoko Hashimoto, Maki Kawamura, and Chiharu Minami for technical assistance.

REFERENCES

1. Di Bisceglie AM. Hepatitis C and hepatocellular carcinoma. Hepatology 1997;26: 34S–8S.
2. Ikeda K, Saitoh S, Suzuki Y, et al. Disease progression and hepatocellular carcinogenesis in patients with chronic viral hepatitis: a prospective observation of 2215 patients. J Hepatol 1998;28:930–8.

3. Kim CM, Koike K, Saito I, Miyamura T, Jay G. HBx gene of hepatitis B virus induces liver cancer in transgenic mice. Nature 1991;351:317–20.
4. Koike K, Moriya K, Iino S, et al. High-level expression of hepatitis B virus HBx gene and hepatocarcinogenesis in transgenic mice. Hepatology 1994;19:810–9.
5. Moriya K, Fujie H, Shintani Y, et al. The core protein of hepatitis C virus induces hepatocellular carcinoma in transgenic mice. Nat Med 1998;4:1065–7.
6. Lerat H, Honda M, Beard MR, et al. Steatosis and liver cancer in transgenic mice expressing the structural and nonstructural proteins of hepatitis C virus. Gastroenterology 2002;122:352–65.
7. Matsubara K, Tokino T. Integration of hepatitis B virus DNA and its implications for hepatocarcinogenesis. Mol Biol Med 1990;7:243–60.
8. Hildt E, Saher G, Bruss V, Hofschneider PH. The hepatitis B virus large surface protein (LHBs) is a transcriptional activator. Virology 1996;225:235–9.
9. Meyer M, Caselmann WH, Schluter V, Schreck R, Hofschneider PH, Baeuerle PA. Hepatitis B virus transactivator MHBst: activation of NF-kappa B, selective inhibition by antioxidants and integral membrane localization. EMBO J 1992;11:2991–3001.
10. Chisari FV, Klopchin K, Moriyama T, et al. Molecular pathogenesis of hepatocellular carcinoma in hepatitis B virus transgenic mice. Cell 1989;59:1145–56.
11. Dunsford HA, Sell S, Chisari FV. Hepatocarcinogenesis due to chronic liver cell injury in hepatitis B virus transgenic mice. Cancer Res 1990;50:3400–7.
12. Hagen TM, Huang S, Curnutte J, et al. Extensive oxidative DNA damage in hepatocytes of transgenic mice with chronic active hepatitis destined to develop hepatocellular carcinoma. Proc Natl Acad Sci USA 1994;91:12808–12.
13. Chisari FV, Ferrari C. Hepatitis B virus immunopathogenesis. Annu Rev Immunol 1995;13:29–60.
14. Cerny A, Chisari FV. Immunological aspects of HCV infection. Intervirology 1994; 37:119–25.
15. Chang KM, Rehermann B, Chisari FV. Immunopathology of hepatitis C. Springer Semin. Immunopathol 1997;19:57–68.
16. Rehermann B, Chisari FV. Cell mediated immune response to the hepatitis C virus. Curr Top Microbiol Immunol 2000;242:299–325.
17. Moriyama T, Guilhot S, Klopchin K, et al. Immunobiology and pathogenesis of hepatocellular injury in hepatitis B virus transgenic mice. Science 1990;248:361–4.
18. Ando K, Moriyama T, Guidotti LG, et al. Mechanisms of class I restricted immunopathology. A transgenic mouse model of fulminant hepatitis. J Exp Med 1993;178: 1541–54.
19. Ando K, Guidotti LG, Wirth S, et al. Class I-restricted cytotoxic T lymphocytes are directly cytopathic for their target cells in vivo. J Immunol 1994;152:3245–53.
20. Franco A, Guidotti LG, Hobbs MV, Pasquetto V, Chisari FV. Pathogenetic effector function of CD4-positive T helper 1 cells in hepatitis B virus transgenic mice. J Immunol 1997;159:2001–8.
21. Nakamoto Y, Guidotti LG, Kuhlen CV, Fowler P, Chisari FV. Immune pathogenesis of hepatocellular carcinoma. J Exp Med 1998;188:341–50.
22. Nakamoto Y, Kaneko S, Fan H, et al. Prevention of hepatocellular carcinoma development associated with chronic hepatitis by anti-fas ligand antibody therapy. J Exp Med 2002;196:1105–11.
23. Kondo T, Suda T, Fukuyama H, Adachi M, Nagata S. Essential roles of the Fas ligand in the development of hepatitis. Nat Med 1997;3:409–13.
24. Nakamoto Y, Guidotti LG, Pasquetto V, Schreiber RD, Chisari FV. Differential target cell sensitivity to CTL-activated death pathways in hepatitis B virus transgenic mice. J Immunol 1997;158:5692–7.
25. Suda T, Takahashi T, Golstein P, Nagata S. Molecular cloning and expression of the Fas ligand, a novel member of the tumor necrosis factor family. Cell 1993;75: 1169–78.
26. Rouvier E, Luciani MF, Golstein P. Fas involvement in Ca(2+)-independent T cell-mediated cytotoxicity. J Exp Med 1993;177:195–200.
27. Anel A, Buferne M, Boyer C, Schmitt-Verhulst AM, Golstein P. T cell receptor-induced Fas ligand expression in cytotoxic T lymphocyte clones is blocked by protein tyrosine kinase inhibitors and cyclosporin A. Eur J Immunol 1994;24:2469–76.
28. Vignaux F, Vivier E, Malissen B, Depraetere V, Nagata S, Golstein P. TCR/CD3 coupling to Fas-based cytotoxicity. J Exp Med 1995;181:781–6.
29. Suda T, Okazaki T, Naito Y, et al. Expression of the Fas ligand in cells of T cell lineage. J Immunol 1995;154:3806–13.
30. Chisari FV, Filippi P, McLachlan A, et al. Expression of hepatitis B virus large envelope polypeptide inhibits hepatitis B surface antigen secretion in transgenic mice. J Virol 1986;60:880–7.
31. Chisari FV, Filippi P, Buras J, et al. Structural and pathological effects of synthesis of hepatitis B virus large envelope polypeptide in transgenic mice. Proc Natl Acad Sci USA 1987;84:6909–13.
32. Wirth S, Guidotti LG, Ando K, Schlicht HJ, Chisari FV. Breaking tolerance leads to autoantibody production but not autoimmune liver disease in hepatitis B virus envelope transgenic mice. J Immunol 1995;154:2504–15.
33. Coligan JE, Kruisbeek AM, Margulies DH, Shevach EM, Strober W. Current Protocols in Immunology. New York: John Wiley & Sons, Inc., 1994.
34. Guidotti LG, Martinez V, Loh YT, Rogler CE, Chisari FV. Hepatitis B virus nucleocapsid particles do not cross the hepatocyte nuclear membrane in transgenic mice. J Virol 1994;68:5469–75.
35. Urase K, Fujita E, Miho Y, et al. Detection of activated caspase-3 (CPP32) in the vertebrate nervous system during development by a cleavage site-directed antiserum. Brain Res Dev Brain Res 1998;111:77–87.
36. Guidotti LG, Ishikawa T, Hobbs MV, Matzke B, Schreiber R, Chisari FV. Intracellular inactivation of the hepatitis B virus by cytotoxic T lymphocytes. Immunity 1996;4:25–36.
37. Guidotti LG, Rochford R, Chung J, Shapiro M, Purcell R, Chisari FV. Viral clearance without destruction of infected cells during acute HBV infection. Science 1999;284: 825–9.
38. Gilles PN, Guerrette DL, Ulevitch RJ, Schreiber RD, Chisari FV. HBsAg retention sensitizes the hepatocyte to injury by physiological concentrations of interferon-gamma. Hepatology 1992;16:655–63.
39. Homann D, Teyton L, Oldstone MB. Differential regulation of antiviral T-cell immunity results in stable CD8+ but declining CD4+ T-cell memory. Nat Med 2001;7:913–9.
40. Lau LL, Jamieson BD, Somasundaram T, Ahmed R. Cytotoxic T-cell memory without antigen. Nature 1994;369:648–52.
41. Murali-Krishna K, Lau LL, Sambhara S, Lemonnier F, Altman J, Ahmed R. Persistence of memory CD8 T cells in MHC class I-deficient mice. Science 1999;286: 1377–81.
42. Kaech SM, Wherry EJ, Ahmed R. Effector and memory T-cell differentiation: implications for vaccine development. Nat Rev Immunol 2002;2:251–62.
43. Perez-Losada J, Balmain A. Stem-cell hierarchy in skin cancer. Nat Rev Cancer 2003;3:434–43.
44. Liang TJ, Rehermann B, Seeff LB, Hoofnagle JH. Pathogenesis, natural history, treatment, and prevention of hepatitis C. Ann Intern Med 2000;132:296–305.
45. Nakamoto Y, Kaneko S. Mechanisms of viral hepatitis induced liver injury. Curr Mol Med 2003;3:537–44.
46. Columbano A, Shinozuka H. Liver regeneration versus direct hyperplasia. FASEB J 1996;10:1118–28.
47. Sell S. Heterogeneity and plasticity of hepatocyte lineage cells. Hepatology 2001;33: 738–50.
48. Coleman WB. Mechanisms of human hepatocarcinogenesis. Curr Mol Med 2003;3: 573–88.
49. Shirota Y, Kaneko S, Honda M, Kawai HF, Kobayashi K. Identification of differentially expressed genes in hepatocellular carcinoma with cDNA microarrays. Hepatology 2001;33:832–40.
50. Xu XR, Huang J, Xu ZG, et al. Insight into hepatocellular carcinogenesis at transcriptome level by comparing gene expression profiles of hepatocellular carcinoma with those of corresponding noncancerous liver. Proc Natl Acad Sci USA 2001;98: 15089–94.
51. Hsu IC, Metcalf RA, Sun T, Welsh JA, Wang NJ, Harris CC. Mutational hotspot in the p53 gene in human hepatocellular carcinomas. Nature 1991;350:427–8.
52. Bressac B, Kew M, Wands J, Ozturk M. Selective G to T mutations of p53 gene in hepatocellular carcinoma from southern Africa. Nature 1991;350:429–31.
53. Kern MA, Breuhahn K, Schirmacher P. Molecular pathogenesis of human hepatocellular carcinoma. Adv Cancer Res 2002;86:67–112.
54. Eferl R, Ricci R, Kenner L, et al. Liver tumor development. c-Jun antagonizes the proapoptotic activity of p53. Cell 2003;112:181–92.

JOURNAL OF VIROLOGY, Mar. 2004, p. 2738–2748 Vol. 78, No. 6
0022-538X/04/$08.00+0 DOI: 10.1128/JVI.78.6.2738–2748.2004

Effect of Interaction between Hepatitis C Virus NS5A and NS5B on Hepatitis C Virus RNA Replication with the Hepatitis C Virus Replicon

Tetsuro Shimakami,[1,2] Makoto Hijikata,[3] Hong Luo,[1,4] Yuan Yuan Ma,[1] Shuichi Kaneko,[2] Kunitada Shimotohno,[3] and Seishi Murakami[1]*

Department of Molecular Oncology, Cancer Research Institute, Kanazawa University,[1] and Department of Gastroenterology, Kanazawa University Graduate School of Medicine,[2] Takara-Machi, Kanazawa, Ishikawa 920-0934, and Department of Viral Oncology, Institute for Virus Research, Kyoto University, Sakyo-Ku, Kyoto 606-8507,[3] Japan, and The Institute of Infectious Diseases, West China Hospital, Sichuan University, Chengdu, Sichuan 610041, China[4]

Received 3 September 2003/Accepted 10 November 2003

Hepatitis C virus (HCV) NS5A has been reported to be important for the establishment of replication by adaptive mutations or localization, although its role in viral replication remains unclear. It was previously reported that NS5A interacts with NS5B via two regions of NS5A in the isolate JK-1 and modulates the activity of NS5B RdRp (Y. Shirota et al., J. Biol. Chem., 277:11149–11155, 2002), but the biological significance of this interaction has not been determined. In this study, we addressed the effect of this interaction on HCV RNA replication with an HCV replicon system derived from the isolate M1LE (H. Kishine et al., Biochem. Biophys. Res. Commun., 293:993–999, 2002). We constructed three internal deletion mutants, M1LE/5Adel-1 and M1LE/5Adel-2, each encoding NS5A which cannot bind NS5B, and M1LE/5Adel-3, encoding NS5A that can bind NS5B. After transfection into Huh-7 cells, M1LE/5Adel-3 was replication competent, but both M1LE/5Adel-1 and M1LE/5Adel-2 were not. Next we prepared 20 alanine-substituted clustered mutants within both NS5B-binding regions and examined the effect of these mutants on HCV RNA replication. Only 5 of the 20 mutants were replication competent. Subsequently, we introduced a point mutation, S225P, a deletion of S229, or S232I into NS5A and prepared cured Huh-7 cells that were cured of RNA replication by alpha interferon. Finally, with these point mutations and cured cells, we established a highly improved replicon system. In this system, only the same five mutants were replication competent. These results strongly suggest that the interaction between NS5A and NS5B is critical for HCV RNA replication in the HCV replicon system.

The hepatitis C virus (HCV) is a major cause of chronic hepatitis around the world (1, 9). Chronic infection with HCV results in liver cirrhosis and often hepatocellular carcinoma (50, 53). HCV is an enveloped positive-strand RNA virus belonging to the genus *Hepacivirus* in the family *Flaviviridae* (44). The HCV RNA genome is ~9.6 kb in length and consists of a 5′ nontranslated region (5′ NTR), a large open reading frame, and a 3′ NTR. The 5′ NTR contains an internal ribosome entry site (IRES) mediating translation of a single polyprotein of ~3,000 amino acid (aa) residues (57, 59). The polyprotein is cleaved by host and viral protease into at least 10 different products (2, 21, 22, 25, 26). The structural proteins core, E1, and E2 are located in the amino terminus of the polyprotein, followed by p7, a hydrophobic peptide with unknown function, and the nonstructural (NS) proteins NS2, NS3, NS4A, NS4B, NS5A, and NS5B (41). The 3′ NTR consists of a short variable sequence, a poly(U)-poly(UC) tract, and a highly conserved X region, and it is critical for HCV RNA replication and HCV infection (17, 34, 65, 66).

HCV is unique among positive-strand RNA viruses in causing persistent infections, and a high mutation rate in E2 allows it to escape host immune surveillance. These phenomena are tightly associated with chronic inflammation of the liver (27, 32, 61, 62). Therefore, HCV RNA replication has been a target for treatment of HCV. NS5B is an RNA-dependent RNA polymerase (RdRp), the central catalytic enzyme in HCV RNA replication. Several recombinant forms of NS5B expressed and purified from insect cells and *Escherichia coli* are available and catalytically active, and studies with purified NS5B proteins provide insight into the biochemical and catalytic properties of NS5B (3, 16, 39, 64). However, the result that NS5B can initiate de novo RNA replication in vitro with both a non-HCV RNA template and an HCV RNA template may reflect the catalytic property of NS5B but not the tight regulation of HCV RNA replication initiation. Studies of HCV RNA replication in vitro have to overcome several difficulties, since replication requires all or most NS proteins and occurs at the membrane where all of the HCV NS proteins are recruited.

A second system used to study HCV RNA replication is the study of HCV RNA replicons in vivo, which utilizes autonomously replicating HCV-derived RNAs. These replicon RNAs have the authentic HCV 5′ and 3′ NTRs. The HCV IRES drives the translation of a selectable marker such as neomycin resistance, and an internal encephalomyocarditis virus IRES directs translation of NS3 to NS5B (38). In vitro-transcribed replicon RNAs are transfected into the human hepatoma cell line Huh-7 by electroporation and placed under selection. The emergence of neomycin-resistant cell colonies is indicative of

* Corresponding author. Mailing address: Department of Molecular Oncology, Cancer Research Institute, Kanazawa University, 13-1 Takara-Machi, Kanazawa, 920-0934 Ishikawa, Japan. Phone: 81-76-265-2731. Fax: 81-76-234-4501. E-mail: semuraka@kenroku.kanazawa-u.ac.jp.

RNA replication. Recently, adaptive mutations that dramatically enhance the ability of HCV RNA to replicate have been identified in NS3, NS4B, NS5A, and NS5B (4, 24, 35, 37, 40). Initially, only the replicon derived from a genotype 1b isolate, HCV-Con1, was replication competent in Huh-7 cells, and adaptive mutations were required for efficient replication (4, 35, 37, 40). Then, several replicon systems derived from a genotype 1b isolate, HCV-N, and a genotype 1a isolate, HCV-H77, were reported to replicate in Huh-7 cells (6, 23, 24, 29). Recently, a replicon system was established which uses an HCV sequence derived from the human T-cell line MT-2C infected with HCV (a genotype 1b isolate, M1LE) in vitro and isolated 50-1 cells replicating subgenomic RNAs with some amino acid mutations (31, 33, 43, 55).

It was previously reported that NS5A and NS5B interact in vitro and in vivo through two independent regions of NS5A and that NS5A modulates the activity of NS5B RdRp through this interaction in vitro in the isolate JK-1 (54). This ability of NS5A to modulate the RdRp activity in vitro may be consistent with the high frequency of adaptive mutations in NS5A which result in a much more efficient RNA replication in Huh-7 cells; however, the biological meaning of the interaction between NS5A and NS5B remains to be addressed in vivo. Here we report a modified HCV RNA replicon system derived from the isolate M1LE by introducing point mutations (S225P, a deletion of S229, and S232I), and curing 50-1 cells of HCV subgenomic RNA replication by interferon (IFN) treatment. By introducing internal deletion and substitution mutations into NS5A, we demonstrate that the regions essential for the interaction between NS5A and NS5B are also critical for HCV RNA replication in using the HCV replicon system.

MATERIALS AND METHODS

Construction of plasmids. pNNRZ2RU (33) harbors a subgenomic replicon derived from MT-2C cells infected with HCV (a genotype 1b isolate, M1LE; GenBank accession no. AB080299), and this plasmid contains cDNA of wild-type M1LE. For convenience, pNNRZ2RU was digested with *Mlu*I and *Bgl*II, and the obtained fragment was inserted into the *Mlu*I and *Bgl*II sites of the vector pGL3Basic (Promega) to create pGL3-*Mlu*I-*Bgl*II. pGL3-*Mlu*I-*Bgl*II was used as an intermediate vector. All mutations were introduced into pGL3-*Mlu*I-*Bgl*II, and then the fragments of pGL3-*Mlu*I-*Bgl*II digested by *Mlu*I and *Bgl*II containing each mutation were reintroduced into the *Mlu*I and *Bgl*II sites of pNNRZ2RU to create each mutant.

M1LE/5Adel-1 was generated by PCR with the primers 5Adel-1 For (containing a *Mlu*I site) and 5A Rev-3 and then inserted into the *Mlu*I and *Nhe*I sites of pGL3-*Mlu*I-*Bgl*II to create pGL3-*Mlu*I-*Bgl*II-5Adel-1. M1LE/5Adel-2 was generated by PCR with overlap extension with the primers 5Adel-2 For, 5A Rev-2, 5Adel-2 Rev, and 5A For-3 and then inserted into the *Nhe*I and *Sac*I sites of pGL3-*Mlu*I-*Bgl*II to create pGL3-*Mlu*I-*Bgl*II-5Adel-2. M1LE/5Adel-3 was generated by PCR with the primers 5A del-3 For (containing a *Nhe*I site) and 5A Rev-2 and then inserted into the *Nhe*I and *Sac*I sites of pGL3-*Mlu*I-*Bgl*II to create pGL3-*Mlu*I-*Bgl*II-5Adel-3.

An alanine scanning method was used to construct NS5A alanine-substituted mutants to minimize the effects of substituted amino acid residues (7). The positions of alanine-substituted clustered mutations (cm) of NS5A are shown in Fig. 2B. To generate M1LE/cm 94, 100, 105, 110, 113, 120, 127, 134, 141, 148, and 155, each mutation was introduced into the *Mlu*I and *Nhe*I sites of pGL3-*Mlu*I-*Bgl*II by site-directed mutagenesis with primers carrying the necessary nucleotide changes to create pGL3-*Mlu*I-*Bgl*II-cm94, -100, -105, -110, -113, -120, -127, -134, -141, -148, and -155, respectively. To generate M1LE/cm 252, 277, 283, 290, 297, 304, 311, 316, 321, and 328, each mutation was introduced into the *Nhe*I and *Sac*I sites of pGL3-*Mlu*I-*Bgl*II by site-directed mutagenesis with primers carrying the necessary nucleotide changes to create pGL3-*Mlu*I-*Bgl*II-cm252, -277, -283, -290, -297, -304, -311, -316, -321, and -328, respectively.

To generate M1LE/S225P and a deletion of S229 (delS229), the point mutations S225P and delS229 were introduced into the *Mlu*I and *Nhe*I sites of pGL3-*Mlu*I-*Bgl*II by site-directed mutagenesis with primers carrying the necessary nucleotide changes to create pGL3-*Mlu*I-*Bgl*II-S225P and -delS229. The point mutation S232I was introduced into the *Mlu*I and *Sac*I sites of pGL3-*Mlu*I-*Bgl*II by site-directed mutagenesis with primers carrying the necessary nucleotide changes to create pGL3-*Mlu*I-*Bgl*II-S232I. To generate the double mutants containing both the point mutation S232I plus an internal deletion mutation or cm, the *Eco*RI fragments of pGL3-*Mlu*I-*Bgl*II-cm94, -100, -105, -110, -113, -120, -127, -134, and -141 were inserted into the *Eco*RI sites of pGL3-*Mlu*I-*Bgl*II-S232I. Because there were no optimal enzyme sites in the others, the point mutation S232I was introduced into the *Mlu*I and *Sac*I sites of pGL3-*Mlu*I-*Bgl*II-5Adel-1, -del-2, -del-3, and -cm148, -155, -252, -277, -283, -290, -297, -304, -311, -316, -321, and -328 by site-directed mutagenesis with primers carrying the necessary nucleotide changes.

To create double mutants containing both the point mutation S225P plus an internal deletion mutation or cm (cm 252, 277, 283, 290, 297, 304, 311, 316, 321, and 328), the *Nhe*I and *Sac*I fragments of pGL3-*Mlu*I-*Bgl*II-5Adel-2, -5Adel-3, -cm252, -277, -283, -290, -297, -304, -311, -316, -321, and -328 were introduced into the *Nhe*I and *Sac*I sites of pGL3-*Mlu*I-*Bgl*II-S225P.

To generate M1LE/5B-VDD, a point mutation changing the GDD motif of NS5B to VDD was introduced at the *Nde*I and *Sma*I sites of pGL3-*Mlu*I-*Bgl*II by site-directed mutagenesis with primers carrying the necessary nucleotide changes to create pGL3-*Mlu*I-*Bgl*II-5B-VDD.

All of the mammalian expression vectors were derived from pSG5UTPL (36). The vector pNKFLAG (49) was used to express amino-terminally FLAG-tagged proteins. The vector pNKGST (49) was used to express glutathione *S*-transferase (GST)-fused proteins.

pNNRZ2RU was subcloned by PCR with the primers NS5A For, NS5A Rev, NS5B For, and NS5B Rev. NS5A For contains an artificial initiation codon downstream of the *Mun*I site, and NS5B For contains one artificial initiation codon downstream of the *Sac*I site. NS5A Rev contains a *Bgl*II site, and NS5B Rev contains a *Bam*HI site. Full-length NS5A was subcloned into the *Eco*RI and *Bam*HI sites of pNKFLAG to create pNKFLAG-5A/wild, and full-length NS5B was subcloned into the *Sac*I and *Bam*HI sites of pNKGST to create pNKGST-5B/wild.

To create NKFLAG-5A/del-1, and -cm94, -100, -105, -113, -120, -127, -134, -141, -148, and -155, the *Mlu*I and *Nhe*I fragments of pGL3-*Mlu*I-*Bgl*II mutants were introduced at the *Mlu*I and *Nhe*I sites of pNKFLAG-5A/wild. To create NKFLAG-5A/del-2, /del-3, -cm252, -277, -283, -290, -297, -304, -311, -316, -321, and -328, the *Nhe*I and *Sac*I fragments of pGL3-*Mlu*I-*Bgl*II mutants were inserted into the *Nhe*I and *Sac*I sites of pNKFLAG-5A/wild.

The sequences of all of the constructs were confirmed by the dideoxy sequence method. The main primers used for plasmid construction are shown in Table 1.

In vitro transcription and purification of RNA. Plasmids were linearized with *Xba*I and purified by passage through a column (PCR purification kit; Qiagen) prior to transcription. RNA was synthesized with T7 MEGAScript reagents (Ambion) by following the manufacturer's directions, and the reaction was stopped by digestion with RNase-free DNase. The synthesized RNA was passed

TABLE 1. Sequences of primers used in the present study

Primer	Sequence (5′–3′)
5Adel-1 For	ATATATCAACGCGTACCCGGCGTGTAAACCTCTCCTACGG
5Adel-2 For	GTGGAGTCAGAGAACGTTCCTCCGGTGGTACACGGGTGCCCA
5Adel-2 Rev	TACCACCGGAGGAACGTTCTCTGACTCCACGCGGGTGATGTT
5Adel-3 For	ATATATATGCTAGCCAGTTGAAGGTAGTAATTCTGGACTCTTTC
5A For-3	ATCCTTCCCACATTACAGCA
5A Rev-2	CTCAACGTCGGATCCCTTGT
5A Rev-3	GGTCAGCGTCCGGGGAGTCATG
NS5A For	ATATCAATTGCATGTCCGGCTCGTGGCTAAGGGATATT
NS5A Rev	ATATAGATCTGCAGCAGACGACGTCCTCACTAGCCTC
NS5B For	TATCGAGCTCGATGTCAATGTCCTACTCATGGACAGGT
NS5B Rev	ATATGGGATCCCCGGTTGGGGAGCAGGTAGATGCCTAC

through a column (RNeasy mini kit; Qiagen) and dissolved in RNase-free water. The concentration was determined by measuring the optical density at 260 nm, and RNA integrity was checked by nondenaturing agarose gel electrophoresis.

RNA transfection and selection of G418-resistant cells. Subconfluent Huh-7 cells were trypsinized, washed once with phosphate-buffered saline (PBS) (−), and resuspended at 10^7 cells/ml in OPTI-MEM (Gibco-BRL, Invitrogen Life Technologies). Then, 10 to 1,000 ng of transcript was adjusted with total RNA from naive Huh-7 cells to a final amount of 10 μg, which was mixed with 400 μl of the cell suspension in a cuvette with a gap width of 0.4 cm (Bio-Rad). The mixture was immediately transfected into Huh-7 cells by electroporation with GenePulser II system (Bio-Rad) set to 270 V and 975 μF. Following 10 min of incubation at room temperature, the cells were transferred into 10 ml of growth medium and then seeded into a 10- or 15-cm-diameter cell culture dish. For the selection of G418-resistant cells, the medium was replaced with fresh medium containing 0.5 to 1 mg of G418 (Geneticin; Gibco-BRL, Invitrogen Life Technologies)/ml after 24 to 48 h and the medium was changed twice a week. Four weeks after transfection, colonies were stained with Coomassie brilliant blue (0.6 g/liter in 50% methanol–10% acetic acid).

IFN treatment. To stop the replication of HCV subgenomic RNA, 50-1 cells were treated with 10,000 U of IFN-α2b (kindly provided by Schering-Plough)/ml in the absence of G418. After 2 weeks of IFN treatment, the absence of HCV RNA was determined from the results of Northern hybridization, reverse transcription-PCR, and sensitivity to G418.

Cell culture. We used two kinds of Huh-7 cells, one derived from our own laboratory's original Huh-7 cell line, designated Huh-7-DMB, and the cured clone of 50-1 cells, designated Huh-7-KV-C. Both types of Huh-7 cells were grown in Dulbecco's modified Eagle's medium (Gibco-BRL, Invitrogen Life Technologies) supplemented with 10% fetal bovine serum, 2 mM L-glutamine, nonessential amino acids, 100 U of penicillin, and 100 μg of streptomycin.

Preparation of cell extracts, coprecipitation with glutathione resin, and Western blot analysis. The transient transfection of COS1 cells was carried out by using the calcium-phosphate method. The cells were harvested, washed with PBS (−), and sonicated in PBS lysis buffer [PBS (−) containing 250 mM NaCl, 1.0% Triton X-100, 1 mM EDTA, and 1 mM dithiothreitol] with 10 mg (each) of aprotinin and leupeptin per ml. Total cell lysate was diluted 10-fold with PBS lysis buffer, mixed with 40 μl of glutathione-Sepharose 4B beads (glutathione resin) (Amersham Biosciences), and then incubated for 3 h on a rotator in a cold room. After an extensive wash with PBS (−) containing 1.0% Triton X-100, the bound proteins were eluted, fractionated by sodium dodecyl sulfate (SDS)–10% polyacrylamide gel electrophoresis (PAGE), transferred onto nitrocellulose membranes, and subjected to Western blot analysis with anti-FLAG monoclonal antibody. The proteins were visualized by enhanced chemiluminescence according to the manufacturer's instructions (Amersham Biosciences). The nitrocellulose membranes used for Western blot analysis with anti-FLAG monoclonal antibody were reprobed with anti-GST monoclonal antibody (Zymed Laboratories) according to the manufacturer's instructions (Amersham Biosciences).

RESULTS

Interaction between NS5A and NS5B. It was previously reported that NS5A and NS5B associate through two discontinuous regions of NS5A (aa 105 to 162 and 277 to 334) and that NS5A weakly stimulates the activity of NS5B RdRp in vitro initially (at a molar ratio to NS5B of less than 0.1) and then inhibits the activity in a dose-dependent manner (54). To examine the effect of this interaction on HCV RNA replication, we used an HCV RNA replicon system derived from the isolate M1LE and 50-1 cells (33). We prepared a hybrid replicon of JK-1 and M1LE which harbors the JK-1 sequence from aa 92 (*Mlu*I site) of NS5A to the end of NS5B. However, the hybrid replicon did not produce any G418-resistant colony with the Huh-7 cell line (data not shown), so we constructed various mutated versions of NS5A of the RNA replicon derived from M1LE.

First, we confirmed whether the association between NS5A and NS5B through the two discontinuous regions of NS5A occurs with the sequence derived from M1LE. COS1 cells were transiently cotransfected with mammalian expression vectors, pNKFLAG-5A/wild, /del-1, /del-2, and /del-3; pNKGST or pNKGST-5B/wild; and the cell lysates were subjected to a GST pull-down assay. pNKFLAG-5A/wild encodes the full-length and wild-type NS5A proteins of M1LE. pNKFLAG-5A/del-1 encodes the internally deleted NS5A protein missing aa 94 to 162, a deletion 11 aa longer than that reported for JK-1 for the convenience of mutagenesis (aa 105 to 162). pNKFLAG-5A/del-2 encodes the internally deleted NS5A protein missing aa 277 to 334, the same region reported for JK-1. pNKFLAG-5A/del-3 encodes the internally deleted NS5A protein missing aa 235 to 276, a region nonessential for the interaction with NS5B in JK-1. pNKGST-5B/wild encodes the full-length and wild-type NS5B proteins of M1LE, and pNKGST encodes only a GST protein. Under conditions in which the expression levels of FLAG-NS5A proteins (input) were similar and the recovery of the GST-NS5B proteins was almost the same (Fig. 1A, lanes 1 to 5, and C, lanes 2 to 5), coprecipitated NS5A proteins (output) were examined (Fig. 1B, lanes 1 to 5). FLAG-NS5A/wild bound to GST-NS5B (Fig. 1B, lane 2) but not to GST alone (Fig. 1B, lane 1). This result demonstrates that NS5A and NS5B also interact not only in JK-1 but also in M1LE in vivo. Very little FLAG-NS5A/del-1 or /del-2 was recovered (Fig. 1B, lane 3 and 4); however, FLAG-NS5A/del-3 was efficiently pulled down (Fig. 1B, lane 5). When larger amounts of proteins were used for this assay, both FLAG-NS5A/del-1 and /del-2 were weakly detected in the fraction pulled down with GST-NS5B but much significantly weaker than FLAG-5A/wild and /del-3. These results demonstrate that aa 94 to 162 (defined as region 1) and aa 277 to 334 (region 2), but not aa 235 to 276 (region 3), of NS5A seem to be essential for binding NS5B in M1LE as observed in JK-1.

Effect of binding NS5B on HCV RNA replication. To examine the effect of the interaction between NS5A and NS5B on HCV RNA replication in the replicon system, we prepared three kinds of internal deletion mutants, M1LE/5Adel-1, M1LE/5Adel-2, and M1LE/5Adel-3, missing regions 1, 2, and 3 of NS5A, respectively (Fig. 2). M1LE/5Adel-1 and M1LE/5Adel-2 are impaired in their binding to NS5B, but M1LE/5Adel-3 is not. As a negative control, we prepared M1LE/5B-VDD, in which the GDD motif of NS5B was mutated to VDD.

FLAG-tagged wild-type and internally deleted NS5A proteins were efficiently expressed in transiently transfected COS1 cells (Fig. 3). When wild-type M1LE and M1LE/5Adel-3 were transfected by electroporation into our laboratory's Huh-7 cell line, Huh-7-DMB, G418-resistant colonies emerged after selection at a concentration of 1 mg/ml. In the case of M1LE/5Adel-3, the number of G418-resistant colonies was about seven times fewer than in wild-type M1LE. In contrast, no colonies emerged when M1LE/5Adel-1, M1LE/5Adel-2, and M1LE/5B-VDD were transfected into Huh-7-DMB cells, indicating that both of the NS5B-interacting regions of NS5A are critical for HCV RNA replication (Fig. 4). The fact that M1LE/5Adel-3 was replication competent but less efficient than the wild type in Huh-7-DMB cells may reflect some roles of region 3 in HCV RNA replication or a conformational change introduced by the internal deletion (see Discussion).

To minimize the effect of the internal deletion and further delineate the sequence(s) critical for HCV RNA replication, we used the alanine-scanning method (7). All residues of the two regions were scanned by introducing alanine substitution

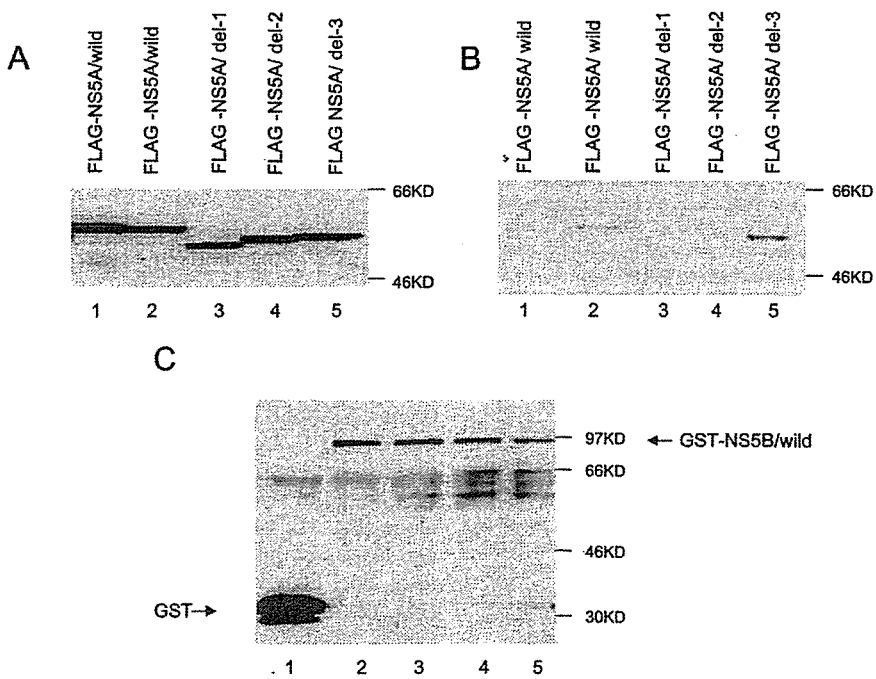

FIG. 1. Interaction between NS5A and NS5B of the isolate HCV M1LE and the regions essential for this interaction. COS1 cells were transiently cotransfected with mammalian expression vectors expressing FLAG-NS5A proteins (lanes: 1 and 2, wild type; 3, internal deletion mutant 1; 4, internal deletion mutant 2; 5, internal deletion mutant 3) and GST protein alone (lane 1) or GST-NS5B proteins (lanes 2, 3, 4, and 5). (A) Input of FLAG-NS5A proteins. Total lysates were fractionated by SDS–10% PAGE and subjected to Western blot analysis with anti-FLAG monoclonal antibody. (B) Output of FLAG-NS5A proteins. Coprecipitants by glutathione resin were washed with PBS (−) containing 1.0% Triton X-100, fractionated by SDS–10% PAGE, and subjected to Western blot analysis with anti-FLAG monoclonal antibody. (C) Recovery of GST or GST-NS5B proteins. The nitrocellulose membrane used for Western blot analysis of coprecipitants with anti-FLAG antibody was reprobed with anti-GST antibody. Molecular masses (in kilodaltons) are indicated to the right of each panel.

cm in addition to one cm mutant within region 3 as a control (Fig. 2). All of these cm mutants in FLAG-tagged forms, 10 in region 1, 9 in region 2, and 1 in region 3, were similarly expressed in transiently transfected COS1 cells (Fig. 3). When these 20 mutants were transfected by electroporation into Huh-7-DMB cells, only M1LE/cm 252, 277, 283, 290, 297, and 304 were found to be replication competent, although less so than wild-type M1LE. All other mutants were replication incompetent (Fig. 5). The regions of cm 252, 277, 283, 290, 297, and 304 are predicted to form a helical structure by DNASIS-Mac, version 3.2 (Hitachi Software Engineering Co.). The competence of replication may be due to this original structure (see Discussion). To rule out this possibility, we constructed another cm mutant, M1LE/cm 110. In this mutant, the region from aa 110 to 117 of NS5A is predicted to form a helical structure, were all changed to alanines, and after the transfection into Huh-7-DMB cells, no colonies emerged (data not shown). These results support the notion that the inability of the internal deletion mutants, M1LE/5Adel-1 and M1LE/5Adel-2, to replicate is due not to conformational change induced by the deletions but to the absence of interaction between NS5A and NS5B. It is also unlikely that these results are due to an increased cytotoxicity associated with the mutant NS5As, because we observed no decrease in transfection efficiency or ability to establish colonies by using the plasmid encoding a drug resistance marker along with the wild or the mutant NS5A protein (data not shown).

Improvement in the HCV replicon system. The results clearly showed that two discontinuous regions of NS5A are essential for HCV RNA replication by using the HCV replicon system with Huh-7-DMB cells; however, the number of G418-resistant colonies per microgram of transfected RNA was much smaller than previously reported (24, 29, 35, 37). It remains unclear whether some mutants were replication competent but too inefficient to be detected in the system we applied. Therefore, we tried to improve the assay system in two ways, by the introduction of point mutations to NS5A and by the selection of Huh-7 cells cured of HCV RNA replication by IFN treatment.

We constructed three mutants, M1LE/S225P, M1LE/delS229, and M1LE/S232I, harboring the point mutation S225P (35), a deletion of S229 (delS229) (24), and S232I (4), respectively, all defined as adaptive mutations in other HCV replicon systems (Fig. 2). Next, the 50-1 cells, an HCV subgenome-replicating subclone, were cured of HCV RNA by treatment with IFN for 2 weeks (as described in Materials and Methods), and then the absence of HCV RNA was determined from the results of Northern hybridization, reverse transcription-PCR, and sensitivity to G418 (data not shown). The 50-1 cells cured of HCV RNA by treatment with IFN, designated

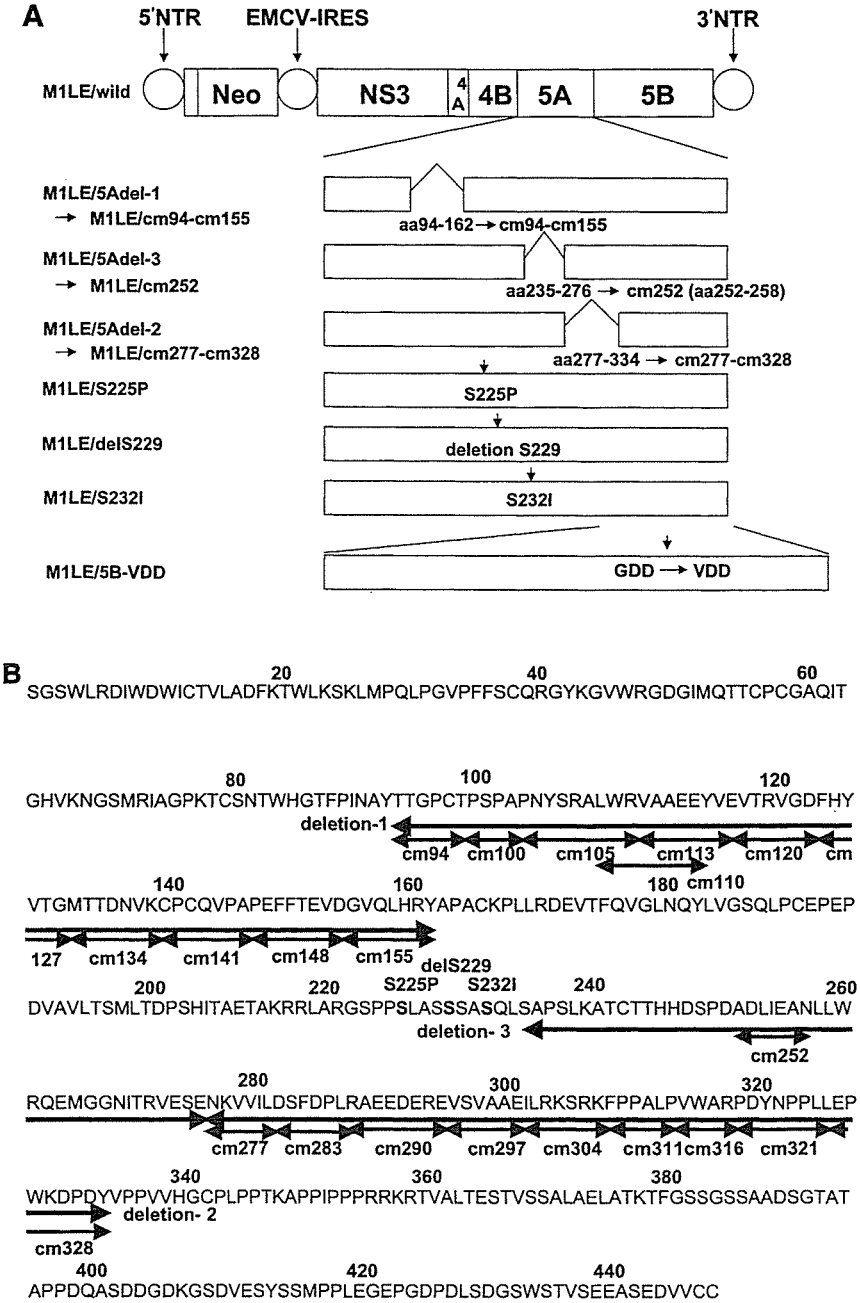

FIG. 2. (A) Schematic presentation of HCV mutant replicons used in this study. Wild-type M1LE contains the HCV M1LE wild-type sequence. M1LE/5Adel-1, M1LE/5Adel-2, and M1LE/5Adel-3 encode internal deletions of NS5A missing aa 94 to 162 (region 1), aa 277 to 334 (region 2), and aa 235 to 276 (region 3), respectively. All amino acids within region 1 were replaced with alanines, and 11 cm mutants were prepared. All amino acids within region 2 were replaced, and 9 cm mutants were prepared. The aa 252 to 258 within region 3 were replaced, and M1LE/cm 252 was prepared. The point mutation S225P, a deletion of S229, and S232I were introduced into wild-type M1LE, and then M1LE/S225P, M1LE/delS229, and M1LE/S232I were prepared. M1LE/5B-VDD encodes NS5B in which the GDD motif was mutated to VDD. (B) Summary of the NS5A mutations. This figure shows the entire amino acid sequence of NS5A of M1LE and the positions of mutations. Numbering starts from the beginning of NS5A. Internal deletions 1, 2, and 3, and point mutations S225P, delS229, and S232I, and cm 252 were introduced as described for panel A. All amino acids within region 1 were replaced with alanines, and then M1LE/cm 94, 100, 105, 110, 113, 120, 127, 134, 141, 148, and 155 were prepared. All amino acids within region 2 were replaced with alanines, and M1LE/cm 277, 283, 290, 297, 304, 311, 316, 321, and 328 were prepared. The positions of the substituted amino acids in each cm mutant are shown in panel B.

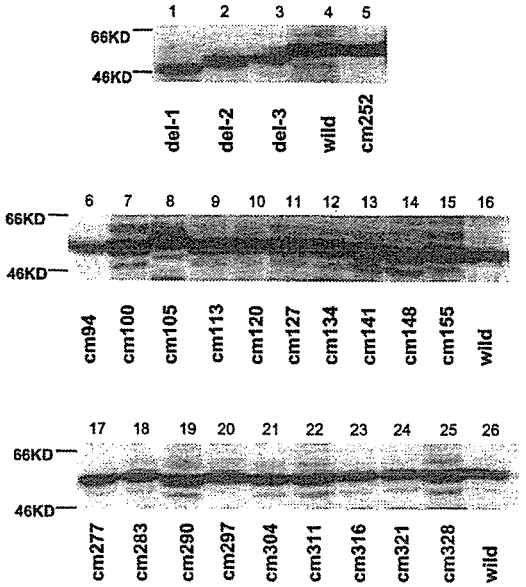

FIG. 3. Efficient translation of mutant FLAG-NS5As. COS1 cells were transiently transfected with mammalian expression vectors expressing FLAG-NS5A proteins that were prepared as described in Materials and Methods. Lanes: 4, 16, and 26, wild type; 1, internal deletion 1; 2, internal deletion 2; 3, internal deletion 3; 5, cm 252; 6, cm 94; 7, cm 100; 8, cm 105; 9, cm 113; 10, cm 120; 11, cm 127; 12, cm 134; 13, cm 141; 14, cm 148; 15, cm 155; 17, cm 277; 18, cm 283; 19, cm 290; 20, cm 297; 21, cm 304; 22, cm 311; 23, cm 315; 24, cm 321; 25, cm 328. Total lysates were fractionated by SDS–10% PAGE and subjected to Western blot analysis with anti-FLAG monoclonal antibody. Molecular masses (in kilodaltons) are indicated to the left of the panels.

Huh-7-KV-C, were evaluated. Wild-type and these mutant HCV replicons were transfected into Huh-7-DMB and Huh-7-KV-C cells. In Huh-7-DMB cells, M1LE/S225P and MlLE/S232I actually increased the efficiency of transduction to some extent, but M1LE/delS229 did not (Fig. 6A). M1LE/S232I was the most effective. In Huh-7-KV-C cells, interestingly, no colonies emerged after selection with G418 when wild-type M1LE was transfected, whereas in the case of M1LE/S225P, delS229, and S232I, 2,500, 3,000, and 25,000 colonies/μg of RNA emerged, respectively (Fig. 6B). These results indicate that two point mutations, S225P and S232I, can be categorized as the adaptive mutations in the isolate M1LE and that the cells cured of HCV RNA by treatment with IFN, Huh-7-KV-C, show higher permissiveness for M1LE/S225P, delS229, and S232I than Huh-7-DMB cells. In this way, we established highly improved replicon systems.

Delineation of important sequences of NS5A for HCV RNA replication. To examine the effect of internal deletions and alanine substitutions on HCV RNA replication with this improved replicon system, double mutants with S232I plus internal deletion mutations or alanine-substituted cm's in M1LE were constructed and transfected into Huh-7-DMB and Huh-7-KV-C cells by electroporation. After G418 selection, in Huh-7-DMB cells, some 400 to 1,000 colonies/μg of RNA emerged with the double mutants of M1LE/S232I plus cm 252, 277, 283, 297, and 304, but only about 100 colonies/μg of RNA emerged with the double mutant M1LE/S232I plus cm 290. No colonies emerged with the double mutant M1LE/S232I plus other cm's, del-1, del-2, and del-3 (Fig. 7; data not shown for Huh-7-KV-C cells). The double mutant M1LE/S232I plus cm 110 was also replication incompetent in Huh-7-DMB cells. To further examine the replication competence of these mutants, double mutants of M1LE/S225P plus an internal deletion mutation or cm were constructed and then transfected into Huh-7-DMB cells. The results were almost the same as those with the double mutants with S232I, although the efficiencies of these mutants were around one-half of those with S232I (Fig. 8). The similar results in the double mutants with S225P were obtained with Huh-7 KV-C cells (data not shown). The replication-defective property of the mutants with deletions of regions 1 and 2, the cm mutants within region 1, and the cm mutants in the C-terminal part of region 2 was also observed with both Huh-7-DMB and Huh-7-KV-C cells, indicating that the replication incompetence of these mutants is not due to the low efficiency of the original assay system. The cm mutants at the N-terminal part of region 2, cm 277, 283, 290, 297, and 304, were replication competent in the absence of the adaptive mutation in Huh-7-DMB cells and also in the presence of the adaptive mutation in Huh-7-DMB and Huh-7-KV-C cells to some extent. Taken together, these results suggest that the interaction with NS5B through regions 1 and 2, probably through its C-terminal part, is also essential for HCV RNA replication. We examined the interaction between cm mutants of FLAG-NS5A and GST-NS5B, but the difference among wild-type and cm mutants was weak in the pull-down assay. Differential binding would be possible if the two partner proteins were lower in concentration or together with other NS proteins, as those occur in vivo in HCV-RNA-replicating cells.

Interestingly, two quantitative differences were observed with M1LE/5Adel-3, cm 252, and 290 with and without the adaptive mutations. M1LE/5Adel-3 was weakly replication competent in Huh-7-DMB cells but incompetent in Huh-7-DMB and Huh-7-KV-C cells when the adaptive mutations were introduced. In contrast, M1LE/cm 252 was weakly replication competent in Huh-7-DMB cells but as high as that of the other replication-competent cm mutants in the presence of the adaptive mutations in Huh-7-DMB and Huh-7-KV-C cells (data not shown for Huh-7-KV-C cells; see Discussion).

DISCUSSION

HCV NS5A is a viral regulatory protein that modulates viral RNA replication and host processes by interacting directly and indirectly with a variety of host regulatory factors (10, 19, 42, 56, 58, 67). The important role of NS5A in HCV RNA replication has been clearly demonstrated by high or clustered incidence of adaptive mutations in NS5A detected in HCV RNA replicon systems, although the molecular mechanism involved remains unknown (4, 24, 35, 37, 40). Shirota et al. previously reported direct interaction between NS5A and NS5B through two binding regions of NS5A expressed in mammalian cells and in vitro with a purified recombinant and that NS5A could modulate the activity of NS5B RdRp in vitro through this direct interaction (54). Here we demonstrated the critical role of regions essential for the NS5A-NS5B interaction in HCV RNA replication with an HCV subgenomic replicon by introducing several internal deletion mutations into

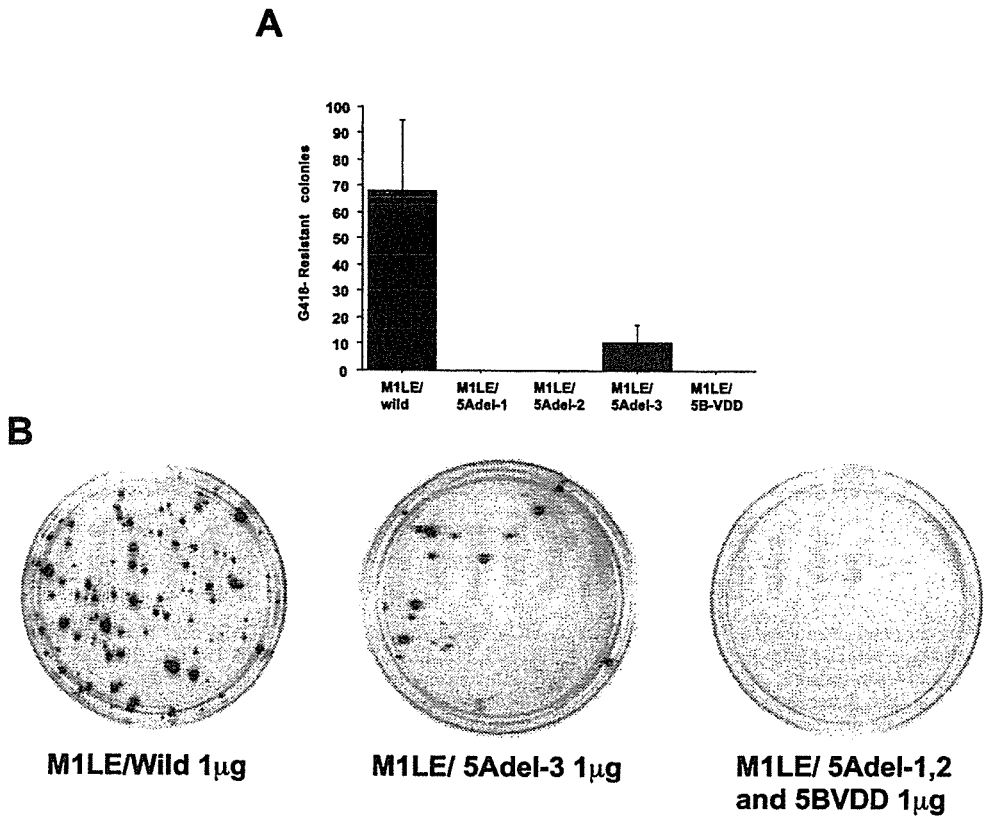

FIG. 4. Effect of internal deletion mutation on HCV RNA replication. Huh-7-DMB cells were transfected with 1 μg of in vitro-transcribed wild-type MILE, 5Adel-1, 5Adel-2, 5Adel-3, and 5B-VDD RNA by electroporation, and G418-resistant cells were selected with a G418 concentration of 1 mg/ml. G418-resistant cell colonies were stained 4 weeks after transfection. (A) This figure shows the mean number of G418-resistant cell colonies isolated per 10-cm-diameter cell culture dish per 1 μg of RNA. Error bars indicate the standard deviations of the results from at least three independent experiments. (B) G418-resistant colonies were visualized by staining cells as described in Materials and Methods.

NS5A. Our results provide clear evidence that NS5A is indispensable for HCV RNA replication probably through its interaction with NS5B, since the mutants missing the NS5B-binding regions, regions 1 and 2, could not produce G418-resistant colonies, but the mutants missing region 3, which is not essential for this interaction, could. The critical role of NS5A in HCV RNA replication in this report is consistent with the previous one that an amino-terminal amphipathic α-helix of NS5A is essential for HCV RNA replication in the replicon system, localizing NS5A to a membrane (13). The use of cm mutants strongly suggests that all of region 1 and the C-terminal part of region 2 are critical for HCV RNA replication. However, it is difficult to exclude the possibility that the substitution of eight amino acids in a row may induce structural change. Then the critical regions defined by cm mutants may simply reflect the structural integrity necessary for the function, although a structural evaluation is difficult at present, since no crystal model of NS5A is available. Further mutational analysis is necessary to test these possibilities.

HCV RNA replication would take place in a distinctly altered membrane structure of the endoplasmic reticulum, a membranous web (12), as recently reported by Gosert et al. (20). All NS proteins might be recruited to the membrane structure via their own membrane association domains or by the help of NS4A in the case of NS3 (8, 13, 20, 28, 30, 51, 52, 63). Recently, Dimitrova et al. (11) reported that all six NS proteins interact with each other through their multiple interacting surfaces. NS5B is HCV RdRp and has been reported to interact with NS proteins and some host proteins. Such interaction(s) may modulate the activity of NS5B RdRp in various ways. The critical role of the homomeric interaction of NS5B in RdRp activity was demonstrated by us and another group (48, 60). Piccininni et al. (47) reported that NS5B interacts with NS3 and NS4B as positive and negative regulators in the replication complex. Previously, it was reported that the direct binding of NS5A and NS5B in the isolate JK-1 weakly stimulated the activity of NS5B RdRp in vitro at first (at a molar ratio to NS5B of less than 0.1) and then inhibited the activity in a dose-dependent manner (54). In the present study, we showed that the two regions of NS5A are important for binding NS5B and are essential for HCV RNA replication in the isolate M1LE by HCV replicon assays. The weak stimulation by NS5A of RdRp activity through the binding of NS5B observed in vitro may reflect the essential role of NS5A in HCV RNA replication, or the interaction between NS5A and NS5B is important for the dynamic assembly of NS proteins in the HCV

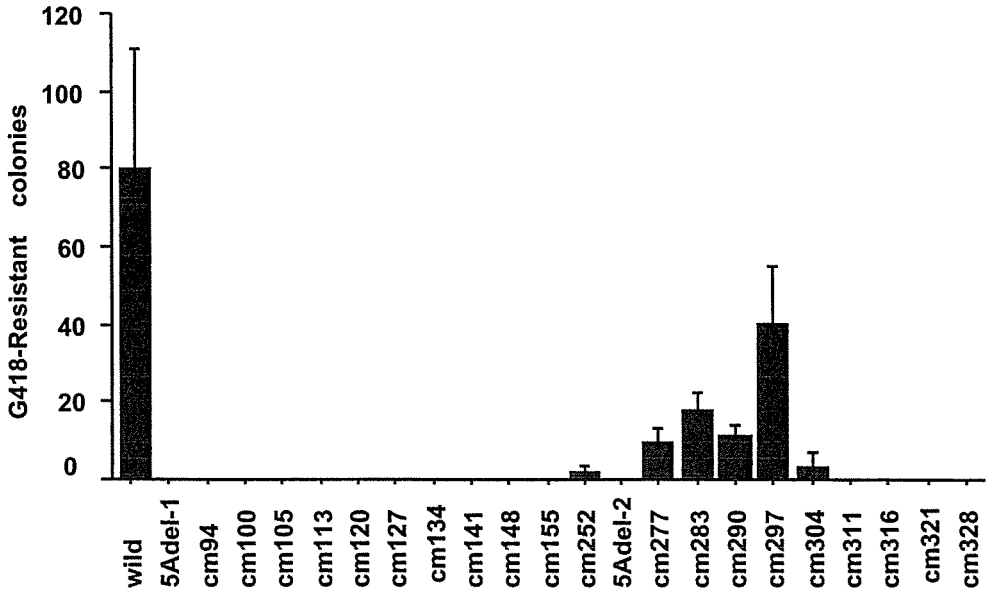

FIG. 5. Effect of clustered alanine-substitution mutations on HCV RNA replication. Huh-7-DMB cells were transfected with 1 μg of in vitro-transcribed wild-type MILE, 5Adel-1, 5Adel-2, and cm 94, 100, 105, 113, 120, 127, 134, 141, 148, 155, 252, 277, 283, 290, 297, 304, 311, 316, 321, and 328 RNA, and G418-resistant cells were selected with a G418 concentration of 0.5 mg/ml. G418-resistant cell colonies were stained 4 weeks after transfection. This figure shows the mean number of G418-resistant cell colonies isolated per 15-cm-diameter cell culture dish per 1 μg of RNA. Error bars indicate the standard deviations of the results from at least three independent experiments.

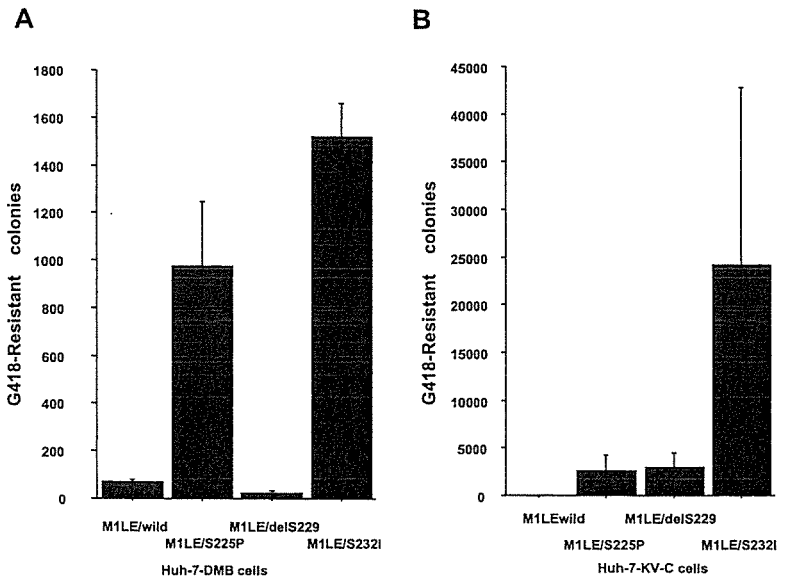

FIG. 6. Effects of three kinds of point mutation, S225P, deletion S229, and S232I, on HCV RNA replication in the Huh-7-DMB and KV-C sublines. 50-1 cells were cured of self-replicating subgenomic RNAs by IFN-α treatment, and then cured 50-1 cells, Huh-7-KV-C, were prepared. Huh-7-DMB and KV-C cells were transfected with 10 ng to 1 μg of in vitro-transcribed wild-type M1LE, M1LE/S225P, M1LE/delS229, and M1LE/S232I RNA. G418-resistant cells were selected with a G418 concentration of 1 mg/ml. G418-resistant cell colonies were stained 4 weeks after transfection. (A) This figure shows the mean number of G418-resistant cell colonies isolated per 10-cm-diameter cell culture dish per 1 μg of RNA when each in vitro-transcribed mutant RNA was transfected into Huh-7-DMB cells. Error bars indicate the standard deviations of the results from at least three independent experiments. (B) This figure shows the mean number of G418-resistant cell colonies isolated per 10-cm-diameter cell culture dish per 1 μg of RNA when each in vitro-transcribed mutant RNA was transfected into Huh-7-KV-C cells. Error bars indicate the standard deviations of the results from at least three independent experiments.

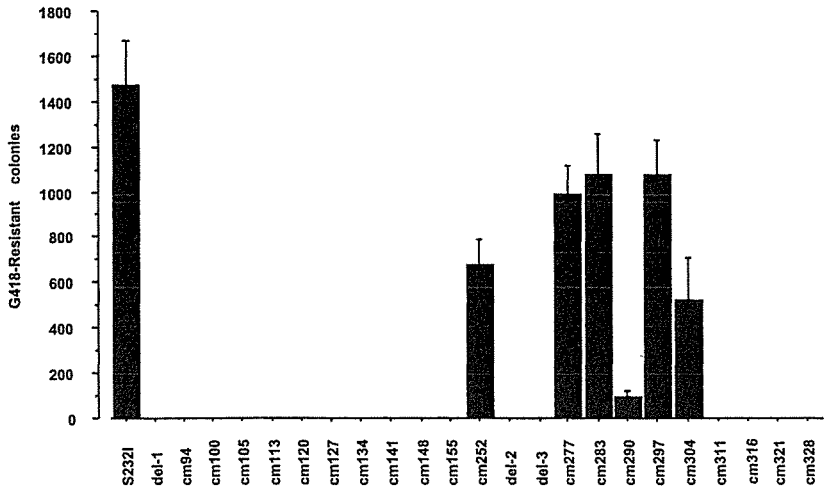

FIG. 7. Effect of M1LE/S232I plus internal deletion mutations or alanine-substitution mutations. Huh-7-DMB cells were transfected with 1 μg of in vitro-transcribed M1LE/S232I plus 5Adel-1, 5Adel-2, 5Adel-3, and cm 94, 100, 105, 113, 120, 127, 134, 141, 148, 155, 252, 277, 283, 290, 297, 304, 311, 316, 321, and 328 RNA. G418-resistant cells were selected with a G418 concentration of 1 mg/ml and stained 4 weeks after transfection. This figure shows the mean number of G418-resistant cell colonies isolated per 10-cm-diameter cell culture dish per 1 μg of RNA. Error bars indicate the standard deviations of the results from at least three independent experiments. The number of G418-resistant cell colonies in M1LE/S232I is derived from the results shown in Fig. 6A.

replication complex. Alternatively, it cannot be excluded that the internal deletion and cm mutants may be defective in other unknown function(s) essential for HCV RNA replication.

Adaptive mutations that increase the efficiency of HCV RNA replication have been accumulated in different HCV replicon systems (4, 24, 35, 37, 40). We introduced several point mutations into NS5A of M1LE and found that two, S232I and S225P, positively affected colony formation as adaptive mutations in two different Huh-7 sublines. Interestingly, a deletion of S229 had an effect distinct from those of the other two mutations, since it was only effective in the cured cells, the KV-C subline. Also, it is noteworthy that wild-type M1LE could not replicate in the Huh-7-KV-C subline. The effect of the deletion of S229 and the replication incompetence of wild-type M1LE may be of interest for the elucidation of the phenotypic or genetic change(s) in the cured cells. In combination with the adaptive mutation, the deletion and cm mutants exhibited distinct phenotypes in HCV RNA replication.

First, the mutant missing region 3 was replication incompetent in the presence of S232I or S225P, which was in contrast

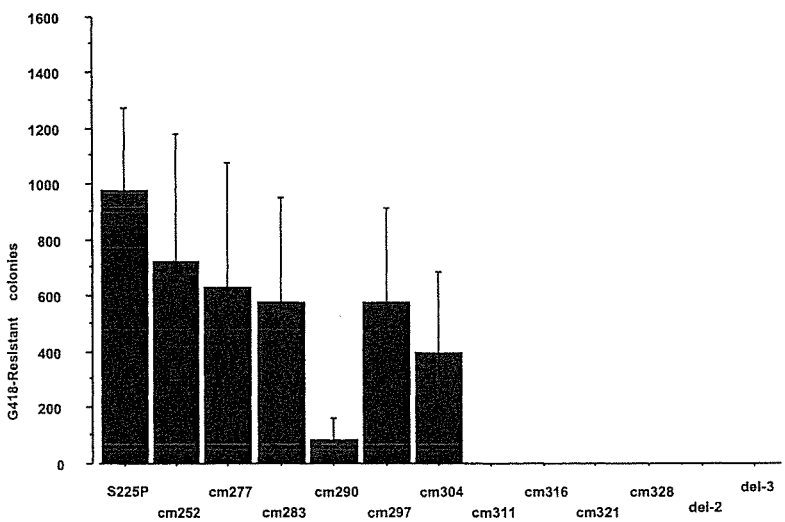

FIG. 8. Effect of M1LE/S225P plus internal deletion mutations or alanine-substitution mutations. Huh-7-DMB cells were transfected with 1 μg of in vitro-transcribed M1LE/S225P plus 5Adel-2, 5Adel-3, and cm 252, 277, 283, 290, 297, 304, 311, 316, 321, and 328 RNA. G418-resistant cells were selected with a G418 concentration of 1 mg/ml and stained 4 weeks after transfection. This figure shows the mean number of G418-resistant cell colonies isolated per 10-cm-diameter cell culture dish per 1 μg of RNA. Error bars indicate the standard deviations of the results from at least three independent experiments. The number of G418-resistant cell colonies in M1LE/S225P is derived from the results shown in Fig. 6A.